

VIRTUAL SURGERY

Development of a surgical simulation tool for the prediction of functional impairment after partial glossectomy

K.D.R. Kappert



VIRTUAL SURGERY

Development of a surgical simulation tool for the prediction of functional impairment after partial glossectomy

Kilian D.R. Kappert
Technical Medicine – Medical Imaging and Intervention
September 2015 – August 2016

Masters Graduation Committee

Chairman and external member

Prof T. Ruers, MD, PhD
Department of surgical oncology
Netherlands Cancer Institute, Amsterdam, The Netherlands
MIRA institute for Biomechanical Engineering and Technical Medicine
University of Twente, Enschede, The Netherlands

Clinical supervisor

Prof A.J.M. Balm, MD, PhD, FACS, FRCS
Department of Head and Neck Oncology and Surgery
Netherlands Cancer Institute, Amsterdam, The Netherlands

Technical Supervisor

F. van der Heijden, PhD
MIRA institute for Biomechanical Engineering and Technical Medicine
University of Twente, Enschede, The Netherlands

Mentor

P.A. van Katwijk, Msc.
MIRA institute for Biomechanical Engineering and Technical Medicine
University of Twente, Enschede, The Netherlands

Additional member

M.J.A. van Alphen, PhD
Department of Head and Neck Oncology and Surgery
Netherlands Cancer Institute, Amsterdam, The Netherlands

Preface

About one and a half years ago Ferdi van der Heijden said: I think you like programming, would you be interested in finding out how to work with Java and biomechanical modelling in a 10 week internship at the Netherlands Cancer Institute? It was not a typical Technical Medicine internship as a large part of the work could be seen as “computer science”. But Ferdi was right, I really liked working at this subject with these tools although it was very challenging. After this small internship I started, without any doubt, on my graduation internship at the NKI. Crucial for this thesis was my visit to the department of Electrical and Computer Engineering at University of British Columbia. Here I was assisted by Sidney Fels, John Lloyd, Antonio Sanchez and others. I couldn’t have done this thesis without their help, so I am very grateful for the hours of help they gave me (and still give, via email). I also want to thank my landlord and roommate Jennifer for the great time we had, and for showing me around Vancouver and its surroundings. I want to thank Fons Balm and Ferdi van de Heijden for giving me the opportunity and motivation to spend two and a half months at the University of British Columbia. I want to thank Maarten van Alpen, Merijn Eskes and Simone van Dijk for their support while I was at the NKI. Last, I want to thank my mother, sister and family for their support, but in particular my dad and granddad whom we have lost last year. Without them I would never have become who I am today, I would have never made the same choices and I wouldn’t have been as happy as I am now.

Summary

Introduction: Prediction of functional consequences of a partial glossectomy can be difficult because of the complex synergistic activities of many muscles and neural structures involved in the swallowing and speech process. Predicting these functional consequences could give both the surgeon and the patient the information they need to choose the right treatment.

Method: In this report a tool to perform surgery on a finite element based biomechanical model of the tongue is presented. The tool enables removal of a volume from the model and suturing of the virtual wound. In addition, scar tissue is added. The biomechanical model itself is an edited version of an existing biomechanical model. To make editing of the biomechanical model possible, the finite element and surface mesh are separated. The surgery tool is validated using real patient cases. From these patient cases, pre and postoperative 3D videos are analysed and compared with the biomechanical tongue, edited by the surgical tool.

Results: The new biomechanical tongue model is comparable with the model on which it is based. Only the Superior longitudinal- and Hyoglossus muscle have different volumes and act slightly different. Patient cases show that the biomechanical model is able to give a qualitative indication about the direction of impairment after surgery. Quantitative comparison is not yet possible because of the restrictions of the measurement method to measure the movement of the patient's tongue.

Conclusion: In this report the next step towards prediction of functional outcome of a glossectomy is made. After personalising the tongue shape, muscles and fibrous tissue this tongue could be implemented in a biomechanical model of the aerodigestive tract to simulate mastication, swallowing and speech.

Index Terms— partial glossectomy, biomechanical model, virtual surgery, virtual therapy, Finite Element Method/Analysis, functional inoperability, ArtiSynth.

Table of contents

1. INTRODUCTION	1
2. METHODS AND MATERIALS	2
2.1 MATERIALS	2
2.2 DEFINITIONS EXPLANATION:	3
2.2.1 <i>Surface mesh</i>	3
2.2.2 <i>FEM model</i>	3
2.3 THE INITIAL MODEL	3
2.4 THE NEW MODEL	4
2.5 MECHANICAL PROPERTIES	5
2.5.1 <i>Passive muscle tissue properties:</i>	5
2.5.2 <i>Active fibre muscles properties (initial model)</i>	5
2.5.3 <i>Active element muscle properties (New model)</i>	5
2.5.4 <i>Physical simulation – forward modelling</i>	5
2.5.5 <i>Physical simulation – inverse modelling</i>	5
2.6 SELECTION METHOD	6
2.7 REMOVAL OF TISSUE AND IMPLEMENTATION OF MUSCLE	8
2.8 CLOSING THE RESECTION AREA	9
2.9 MOTION SIMULATION	9
2.10 VALIDATION BY COMPARISON WITH THE INITIAL MODEL	10
2.11 VALIDATION USING PATIENT CASES	10
2.11.1 <i>Range of Motion measurement</i>	10
2.11.2 <i>Forward simulation</i>	11
2.11.3 <i>Inverse simulation</i>	11
2.11.4 <i>Video inspection</i>	11
3. RESULTS	11
3.1 INITIAL MODEL VERSUS NEW MODEL	11
3.2 PATIENT CASES	15
3.3 PATIENT COMPARISON	16
4. DISCUSSION	17
4.1 THE MODEL	17
4.2 PATIENT COMPARISON	18
5. FUTURE PERSPECTIVE	19
5.1 PERSONALISED TONGUE MESH	19
5.2 PERSONALISED MUSCLE BUNDLES	19
5.3 STIFFNESS & FIBROSIS	19
5.4 IMPROVED FEM STRUCTURE	19
5.5 TECHNIQUES FOR MEASURING PRE AND POSTOPERATIVE TONGUE MOTION	19
5.6 CREATION OF THE COMPLETE AIRWAY STRUCTURE	19
5.7 COMPARISON WITH EXPERTISE OF SURGEON	19
6. REFERENCES	20
Appendix A. Anatomy of the tongue	22
Appendix B. The Virtual Therapy Project	23
Appendix C. The finite element method	24
Appendix D. Finite element meshing techniques	28
Appendix E. Introduction to Artisynth	29
Appendix F. Prospective range of motion Study	31
Appendix G. Surgeon versus biomechanical model	32

1. INTRODUCTION

With an incidence of almost 3000 people a year, head and neck cancers (HNC) take up 2,7% of all new diagnosed cancers in the Netherlands in 2015 and the numbers are growing¹. Around 90% of all HNCs are squamous cell carcinoma's (SCC), a malignancy derived from the surface epithelial cells². Oral cancer is a subgroup of head and neck carcinomas and makes up 17% of this cancer type. It includes the lips, tongue, floor of mouth, alveolar ridges, gingiva, buccal mucosa and hard palate. From each of these subsites a squamous cell carcinoma may arise, most frequently at the lateral border of the tongue and the floor of mouth³. A SCC of the dorsal surface is rare. The 5 year survival rate is only 60%¹. Oral cancers are believed to be a multifactorial disease. Tobacco use is the single biggest risk factor and appears to have a synergistic effect together with alcohol⁴⁻⁷. Dietary habits, occupational activities, socioeconomic status, exposure to external agents and genetic susceptibility are also risk factors⁸. Unlike most Oropharyngeal cancers, oral cancers can easily be detected by oral examination. Techniques that can assist in the detection of cancerous and precancerous lesions are visual auto fluorescence, narrow band imaging and near infrared fluorescence imaging⁴. The preferred treatment for oral SCC's is surgery followed by radiotherapy or chemo radiation in case of an incomplete resection or too narrow tumour resection margins. Surgery often includes a neck dissection as 20% of the patients with a SCC in the oral cavity have several lymph node metastasis⁶. Alternatives to classical surgery, radiation and chemotherapy that can also be applied are CO₂ laser surgery, trans oral robotic surgery and photodynamic therapy. Tumour characteristics such as size, location, extension, histology and stage are important for the choice of treatment. Also age, condition, compliance and the patient's choice are considerations for the choice of treatment⁸.

The best treatment should minimize patient morbidity and thus improve survival and quality of life (QOL). Post-operative QOL depends largely on the patient's ability to swallow, speak or masticate after surgery. This is called the functional outcome. Due to the complexity of the structures, functional outcome of interventions in the oral cavity are often hard to predict. It is difficult to say to which extent these impairments will occur. Surgical removal has a direct influence on the functional outcome regarding swallowing, mastication and speech. But the functional sequelae of radiation and in particular chemo radiation, can also be substantial. Xerostomia and fibrosis are common toxicities of this treatment modality. The choice for a certain treatment is therefore directly correlated to the physician's experience or multidisciplinary board. If there is not a clear insight in the functional outcome after treatment it is hard for the patient to make an appropriate choice for a certain treatment. A term often used by physicians is: "functional inoperability". It is a term to indicate that the expected functional outcome would be unacceptable for the patient. This is not to be confused with anatomical inoperability.

Table 1: list of tongue muscles and their abbreviations.

Extrinsic muscles	Intrinsic muscles
Genioglossus (GG)	Superior longitudinal muscle (SL)
Hyoglossus (HG)	Inferior longitudinal muscle (IL)
Styloglossus (STY)	Transverse muscle (TRANS)
Palatoglossus*	Vertical muscle (VERT)
Geniohyoidus (GH)**	
Mylohyoid Muscle (MH)**	

*The palatoglossus is not simulated in the biomechanical model
 ** These are muscles from the floor of mouth, but are also embedded in the biomechanical models

A tumour is anatomically inoperable if due to removal of vital structures, in case of radical removal of the tumour, the chance of not surviving the operation would be too high. Functional inoperability is a hard threshold in the middle of a grey area. This area is grey because we do not have the tools yet to predict the functional consequences in full detail whereas a small detail can have significant consequences.

Predicting functional consequences is difficult because of the complex synergistic activities of many muscles and neural structures involved in the swallowing and speech process. A lot of different anatomical structures are used and work together during speech or the swallowing action. Especially the tongue is a complex structure. It consists of eight muscles. The muscles and abbreviations that are relevant in this thesis are listed in Table 1. Appendix A will address the anatomy of the tongue in more detail.

Because of this complexity many researchers are challenged to search for prognostic factors of certain functional outcomes without knowing the exact anatomical orientation or tissue properties. Thanks to these reports it is now known that size and location of the tumour are predictors of functional outcome. For example: tumours at the lateral side of the tongue appear to have a less drastic effect on speech than tumours at the floor of mouth⁹. Also, patients have a greater risk on severe swallowing problems if they undergo a tumour resection with adjuvant Radiotherapy. The same applies for patients that have a stage T3 or T4 tumour or have tumours located at the floor of mouth^{10,11}.

Naturally the biggest improvement in function can be seen in the first months after surgery. Speech doesn't significantly improve in the period between 6 and 12 months, but it appears that the articulation function can still improve over the years^{11,12}. Articulation intelligibility is also better in patients not receiving grafts (such as free-flap reconstruction) than in those receiving grafts¹³.

In 2009 A. Kreeft¹⁴ showed that there is no absolute consensus with regard to functional results for most treatments in oral and oropharyngeal cancers. In response to this, the Virtual Therapy project at the Netherlands Cancer Institute (NKI) was started. The project is aimed at finding tools to predict functional loss in order to choose the right treatment for the patient (Appendix B). Recent research within this project showed that not tumour stage but tumour volume is the best indicator for the extent of postoperative functional impairment¹⁵. Other ongoing research already showed that an extensive pre-operative Range Of Motion (ROM) of the tongue has positive prognostic effects on the residual tongue mobility. However the most important aim of the Virtual Therapy project is to create a biomechanical model that is able to predict function loss after treatment of Oral and Oropharyngeal cancers, mainly aimed at the tongue.

In most cases, a biomechanical model is created using the Finite Element Method (FEM). FEM is used in engineering to divide structures in smaller parts wherein stress, strain, motion or temperature can be calculated and subsequently be used for calculation of certain property change of the complete structure (see Appendix C for mathematical details). Creating FEM models of the tongue is not a new idea. FEM creations of the tongue date back to 1975 when S. Kiritani et al.¹⁶ created an elastic system to study the physiological functions of certain intrinsic and extrinsic muscles in speech production. The system was grouped in 14 units which were given a certain force to mimic a certain muscle. For each set of muscle contractions only a few iterations could be calculated. With the computational power of today there are much more possibilities. There are a number of recent studies that have focused on the creation of FEM models of the tongue, but there goals are slightly different. In research of J. Gérard et al. (2006)^{17,18} the main focus was to create a FEM model to study speech production. Also van Alphen et al. (2013)¹⁹ from the Virtual Therapy Project created a FEM model in Matlab completely from scratch. Other studies focused on creating a technically faster and better model of the tongue²⁰. Fujita et al. (2007)²¹ created a personal tongue model specifically for the simulation of a glossectomy. This study gave promising results for the usage of the finite element method to predict functional loss. They used a simple preoperative and postoperative model and compared pre and postoperative motion of the tongue. This method was time consuming, since two pre- and postoperative models needed to be created manually for just one patient. The model was completely based on solely one patient as only one case study was used. Also Buchaillard et al. (2007)²² edited their original model to show the potential of biomechanical modelling for the prediction of functional outcome after surgery. Both a Hemiglossectomy (removal of one complete half of the tongue) and a floor of mouth resection with a free-flap reconstruction were mimicked by changing tissue properties of elements at those specific locations on the model. The reconstructed part was then given different amounts of stiffness to simulate the effect of radiation on the new tissue. Especially the amount of stiffness showed a huge impact on the mobility of the tongue and assumedly also on the ability to speak. This research showed promising results for the use of biomechanical modelling in the prediction of postoperative motion, but it was restricted to changing tissue properties in

certain elements. The aim of this report is to take virtual surgery of the tongue to the next level by creating a surgery tool that is capable of demonstrating each type of resection and subsequently simulate the postoperative tongue motion. This virtual surgery will be done on an edited version of the biomechanical FEM model created in Buchaillard et al (2009)²³, henceforth called the “initial model”. The suturing of a wound has never been simulated on a biomechanical model of the tongue, while in the Netherlands it is common in most surgery’s for patients with a SCC of the tongue¹⁴. Therefore suturing will be embedded in the surgery tool. In addition, postoperative scarring (or fibrosis) effects have to be implemented as scarring is an important factor for postoperative motion impairment. While creating this model also other aspects have to be considered: What modifications are needed to enable editing of the FEM structure in the initial model? How is the resection area selected on a 3D model? What tool is needed to create every resection area while still being easy to use? How can the initial FEM model be edited to simulate the postoperative tongue? How can the resection be closed and how can sutures be simulated? How can scar tissue be implemented in this model? As this is the first step towards detailed virtual surgery, it is not expected that this model will give highly accurate and personalised results. This report will therefore primarily focus on the simulation of the surgery and not yet on the personalization of the biomechanical model. The surgery tool created in this work can eventually be applied on highly accurate and personalised models of the tongue. When the impairment of motion can be simulated successfully, the biomechanical model would ultimately be able to predict functional outcomes such as swallowing, mastication and speech.

Validation of the model is needed to get answers on the following question: is the edited virtual surgery model still comparable to the initial model? Is it possible to simulate a real surgical resection and is the postoperative motion of this model comparable to the postoperative tongue motion of real patients? Data for the pre and postoperative tongue motion of real patient will be acquired from the ongoing research of van Dijk et al.²⁴ Details of this research can be found in Appendix F.

2. METHODS AND MATERIALS

2.1 Materials

The initial tongue model of Buchaillard et al (2009)²³ was converted by Stavness et al²⁵ to work in the ArtiSynth simulation platform. Artisynt is an Application Programming Interface (API) for JAVA created at the University of British Columbia that is aimed at creating and simulating solid and deformable structures in mainly the upper airway²⁶. The surgery tool was also created within the ArtiSynth environment. The Artisynt core is currently at subversion 611. A detailed description on Artisynt can be found in appendix A. MATLAB 2015b was used to send, receive and process data from muscle exciters/movements. MeshLab was used for manually editing mesh models²⁷.

2.2 Definitions explanation:

To understand the method section, it is essential to know the terminology that is used. It is especially complex to read because there will be an interplay between the physical model responsible for the biomechanical simulation and the visual model which translates the biomechanical simulation into a visual representation.

2.2.1 Surface mesh

The visual representation of an 3D object is determined by a surface mesh, consisting of vertices, faces and edges (Figure 1).

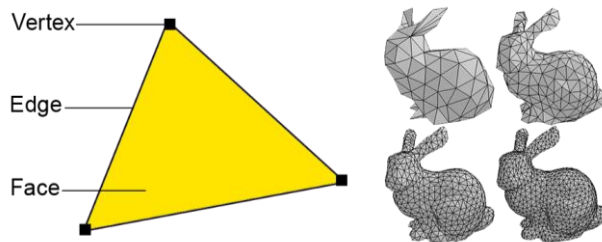


Figure 1: Example of a mesh structure. Image of rabbit mesh acquired from cmap.polytechnique.fr

Using multiple faces a complete structure can be created. Triangular faces are the most practical to work with but it can also be shaped as a square, pentagon etc. All 3D computer animation are based on this principle. It does not have any other functions than to give a representation of a 3D surface. In this report, these surfaces are only used for visualisation.

2.2.2 FEM model

The FEM model is responsible for the biomechanical simulation. It is also a mesh, but it is not the visual representation of the model. In the finite element analysis a 3D object (also objects with other dimensions) is divided into multiple smaller parts, which are called elements.

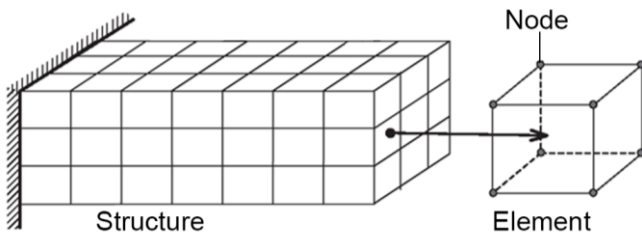


Figure 2: Example of a finite element structure.

An element is a volume demarcated by nodes (Figure 2). When visually representing an element, these nodes function as vertices, but they are more than that. The nodes host the information about the material properties. At each time step a new state for each node is calculated. This can be a state of position, speed or other physical quantities. Via interpolation the new state can be calculated for each position within the element. The FEM model and surface mesh are two completely different aspects of the same object. The FEM model can be visualised by creating vertices and faces that represent a FEM element.

2.3 The Initial Model

The initial model is based on the work of Buchaillard et al (2009)²³ which on itself is based on the model developed by Gerard et al.(2003,2006)^{17,18} This model was constructed using atlas data from the Visible Human Project® for a female subject and the previous work with FEM models of Wilhelms-tricarico (2000)²⁸. The model of Buchaillard differs from the model of Gerard in that it has a changed motor control scheme, a constitutive law for tongue tissue that now also depends on muscle activation, a changed modelling of the hyoid bone and other improvements to the tongue mesh and muscle fibres. The shape of the FEM model is used for the visual representation, which makes the FEM model and the surface mesh visually similar (Figure 3). The muscles are modelled as fibres that are attached to the nodes of the elements. These fibres are spring-like structures with the ability to pull their two endpoint towards each other. The muscle fibres are placed in such a manner, that they resemble the real anatomical location and the movement of the muscles as well as possible (Figure 4).

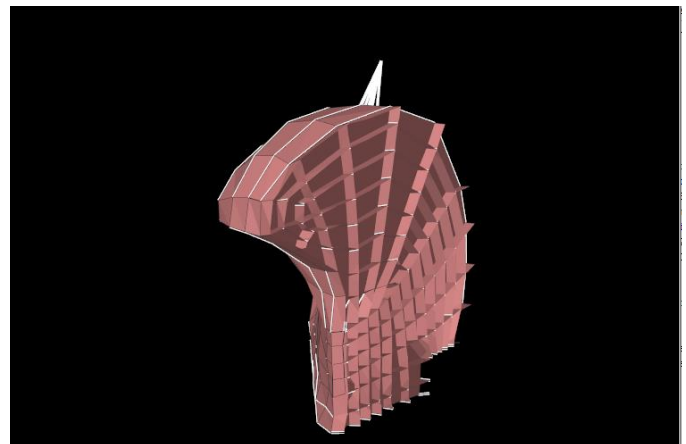


Figure 3: Cross section of the initial model of Buchaillard(2009)²³ in an ArtiSynth simulation.

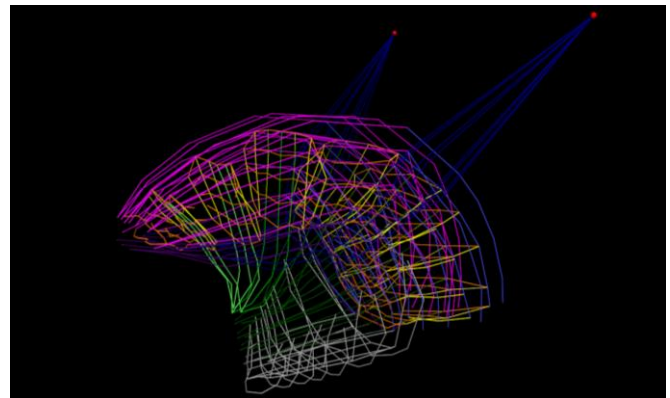


Figure 4: Fibre muscles of the initial model of Buchaillard (2009) in the ArtiSynth environment.

The Genioglossus (GG) muscle does not completely correspond to the real anatomical situation. Normally the GG-anterior emanates from a tendon that is connected to the mandible. Due to the element-resolution of the model, this tendon is not there. Therefore the contact area to the mandible is made larger. The GG is the only tongue muscle which is divided in multiple motor control units with consensus about the partitioning of

motor control units²⁹. The palatoglossus muscle is not included in the model. Finally the model was implemented in the Jaw-tongue-hyoid ArtiSynth-model made in 2011 at the University of British Columbia (UBC)³⁰. The FEM was originally created in ANSYS (commercial FEM software), nevertheless validation showed that displacement errors in the new Artisynth environment (using a demo model of a FEM beam) are at a maximum 0.3%³⁰. As ArtiSynth uses several simplifications compared to ANSYS, such as semi-implicit integration and a lumped mass model, it was noticeably faster than ANSYS. There is also a FEM muscle version of this tongue model. The difference with the fibre muscle model is that the muscle contractions are simulated by contracting the elements itself instead of contracting fibres that are attached to nodes. Because of technical reasons, that will be explained later, the fibre muscle model was used for this report.

2.4 The new model

To take surgery simulations using biomechanical tongue models to the next level, a suitable FEM model was needed. Editing tissue properties of certain areas as done in earlier research was not enough, as primary closing using suturing requires editing the morphology of the model. The initial model was not suitable for editing small and detailed areas. So before a surgery tool could be created the initial model needed to be made suitable to deal with this. To achieve this a couple of methods were tested and evaluated (see Appendix D). The most suitable method can be explained as follows. In the initial model the FEM elements are shaped in such a way that they resemble the shape of the tongue, although that is not required by ArtiSynth. The FEM model, responsible for the deformation and movement of the tongue, can be separate from the surface mesh; the visual representation of the tongue. As long as this surface mesh is located within a FEM structure, it will follow the motion and deformation of this FEM model. Because of computational limitations, the FEM model consists of a finite number of elements in order to retain the ability to simulate motion with an acceptable speed. The benefit of a separate surface mesh and FEM model is that a high resolution surface mesh enables detailed editing, and thus detailed virtual surgery on the surface mesh. A low resolution FEM model can be used to retain the ability to simulate tongue motion near-real time. It is generally difficult to edit a finite element model that has a complex shape (see Appendix D). Therefore a simple method is used where the FEM model is made up by small cubic shaped elements according to the shape of the surface mesh. The FEM model starts as a cube consisting of a given number of elements (Figure 5). The dimension of this cube will be adapted from the 3D diagonal cross section of the tongue mesh. The amount of elements of this cube, depends on both the size of the mesh and the size factor. The size factor is used to define the amount of elements in a certain direction, for example the x direction:

$$Nr. \text{ of elements in } x \text{ direction} = |\mathbf{a} \cdot \hat{\mathbf{x}} * F| \quad (1)$$

with \mathbf{a} the cross diagonal in vector coordinates from the tongue model in meters. $\hat{\mathbf{x}}$ the unit vector in x direction, and F the size factor. A size factor of 400 is used for the model on which surgery is performed. This results in a FEM grid of 31x36x24 elements which are sufficiently small for a virtual resection of a small but significant part of the tongue. Post-surgery models use a size factor of 300 (20x23x18) because 400 appeared to be too slow to simulate a simple manoeuvre within an acceptable simulation time. After removal of the elements that are fully outside the surface mesh, the remaining cubes resemble a shape that is comparable, but slightly larger in volume than the surface mesh (Figure 6). Changing the density to compensate for the increased volume and therefore weight, did not show any change in the motion of the tongue. Therefore the density is not changed to compensate for the increased volume. Because the surface mesh is free from the FEM model, the details of the surface mesh can be improved without making the FEM model more complex and without slowing down the simulation. To improve the visual representation of the tongue and to increase the resolution of the resection, the tongue surface mesh is smoothed using a least squares subdivision surface algorithm from s. Boyé et al (2011)³¹ in the Mesh-editing tool “MeshLab”²⁷ (Figure 5 and Figure 6).

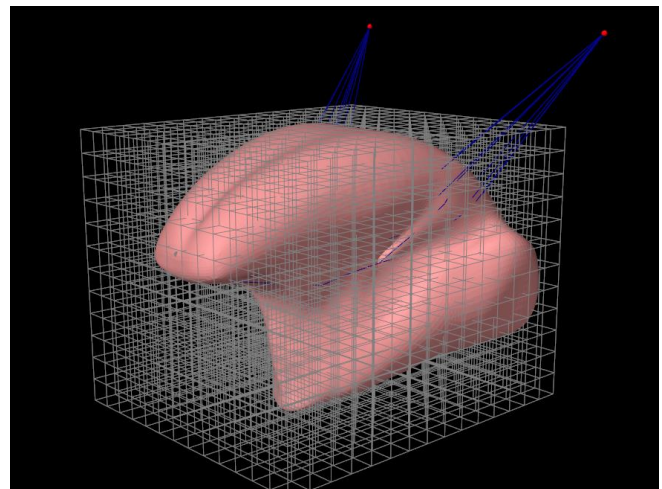


Figure 5: The new mesh of the tongue model. The grid represents the initial set of elements.

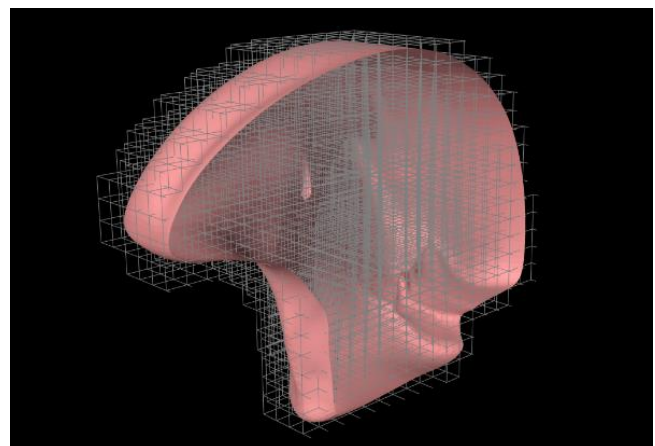


Figure 6: The tongue surface mesh and FEM structure after removing elements that are not inside the surface mesh.

2.5 Mechanical properties

For the simulation of tongue tissue two different constitutive equations were introduced. One for the passive behaviour of tongue tissue and the other for the stress/strain relation as an increasing function for muscle activation. These are essentially the same as used in Buchaillard et al. (2009)²³ et al. and Stavness et al. (2011)^{25,30}

2.5.1 Passive muscle tissue properties:

Fung (1993)³² stated that a hyperelastic material seems to be the best type of material to simulate living tissue. When a material is hyperelastic, it is possible to define a function W , the strain energy function. The derivative of W with respect to the strain tensor equals the stress tensor. The function W can be found using the Yeoh strain-energy function:

$$W = c_{10}(\bar{I}_C - 3) + c_{20}(\bar{I}_C - 3)^2 \quad (2)$$

Where \bar{I}_C is the first invariant of the deviatoric component on the left Cauchy-Green tensor and c_{10} and c_{20} are constants that characterize tissue properties. This constitutive law, proposed by Gerard et al. (2005)³³, was derived from experiments with a fresh cadaver. In Buchaillard et al. (2007,2009)^{22,23} this constitutive law was multiplied with a factor of 5.4 so that the tissue stiffness without muscle contraction was comparable with in vivo measurements of Duck et al.³⁴ The same c_{10} and c_{20} as calculated in Buchaillard et al. will be used: 1037 Pa. and 486 Pa. Figure 7 shows the stress strain relationship derived from the Yeoh strain-energy function.

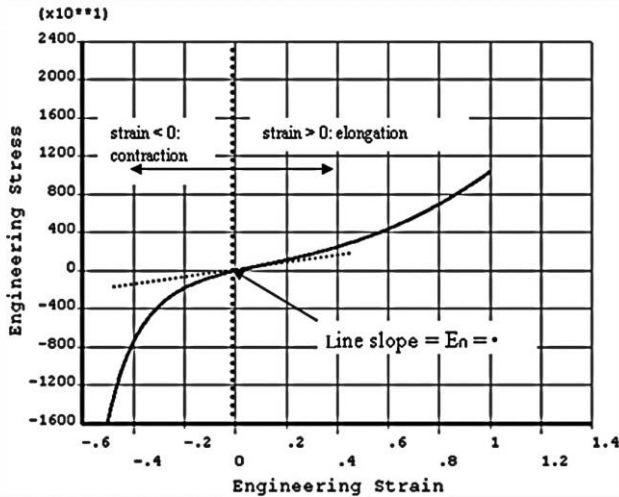


Figure 7: Yeoh second order stress/strain curve acquired from Buchaillard (2007)²² the dotted line is the young's modulus at low strains. Stress is measured in Pa.

2.5.2 Active fibre muscles properties (initial model)

In the initial model, muscles are modelled as fibres. Fibres are spring-like structures between elements. When a muscle contracts the tissue properties change; the tissue becomes stiffer. Tissue stiffening due muscle activation in the initial model is simulated by linearly increasing c_{10} and c_{20} from 1037 Pa. and 486 Pa. with no activation to 10370 Pa. and 4860 Pa. at full activation.

2.5.3 Active element muscle properties (New model)

Because the new model uses element muscles instead of fibre muscles the muscle properties are different. Tissue properties from element muscles in ArtiSynth can change linear with muscle contraction just like the fibre muscles. Another method to simulate the change in tissue stiffness during muscle activation is the method proposed by Blemker et al. (2004)³⁵. This model includes a dilatational term (Ψ_{vol}) and deviatoric stress terms that include along-fibre shear (W_1), along-fibre stretch (W_3) and cross fibre shear (W_2).

$$\Psi = \Psi_{vol}(J) + W_1(\beta_1) + W_2(\beta_2) + W_3(\lambda, \alpha) \quad (3)$$

With J the relative change in volume and β_1 and β_2 strain invariants which give an independent representation to along-fibre and cross-fibre shear³⁶. λ is fibre stretch and α is the muscle activation level. This active term is added in addition to the passive tissue properties.

2.5.4 Physical simulation – forward modelling

To advance the biomechanical model forward in time physical simulation is needed. At each time step a second-order ordinary differential equation (ODE), that is a result of the physics of the mechanical system, needs to be solved. FEM models in ArtiSynth use lumped mass models as these are easy to connect to rigid bodies or mass-spring (e.g. muscle fibre bundles) components. The formula used is newton's second law:

$$\dot{\mathbf{M}}\mathbf{u} = \mathbf{f}(\mathbf{q}, \mathbf{u}, t) \quad (4)$$

With \mathbf{M} the composite mass matrix, \mathbf{q} the positions of the dynamic components, \mathbf{u} the velocities, $\mathbf{f}(\mathbf{q}, \mathbf{u}, t)$ the force of all force effector components and t the time. Constraints are needed to solve the equations. Bilateral constraints include rigid body joints, FEM incompressibility, and point-surface constraints. Unilateral constraints include contact and joint limits. Equation 4 is integrated using a semi-implicit integrator. Other integrators are also available (Appendix E). This leads to the following linear system for determining the velocities for the next time step.

$$\begin{pmatrix} \hat{\mathbf{M}} & -\mathbf{G}^T \\ \mathbf{G} & 0 \end{pmatrix} \begin{pmatrix} \mathbf{U}^{k+1} \\ \boldsymbol{\lambda} \end{pmatrix} = \begin{pmatrix} \mathbf{M}\mathbf{u}^k + h\hat{\mathbf{f}} \\ \mathbf{g} \end{pmatrix} \quad (5)$$

\mathbf{U}^{k+1} are the velocities for the next time step, $\hat{\mathbf{M}}$ is the mass matrix, $\hat{\mathbf{f}}$ is the force matrix, h is the time step size, \mathbf{G} is the matrix of bilateral constrains, $\boldsymbol{\lambda}$ are the impulses that enforce constrains and \mathbf{g} is a term derived from $\hat{\mathbf{G}}$.

2.5.5 Physical simulation – inverse modelling

Inverse simulations are used to compute muscle activations that are needed for a certain movement in a forward simulation. The inverse simulation used in ArtiSynth is based on the tools of I. Stavness³⁷. The input in this case is a certain position in space for a certain part of the tongue. The muscle activation combination to achieve that position is the output of the calculation. Quadratic programming is used to find the muscle combination for a certain movement. Because there are different muscle combinations to achieve the same movement,

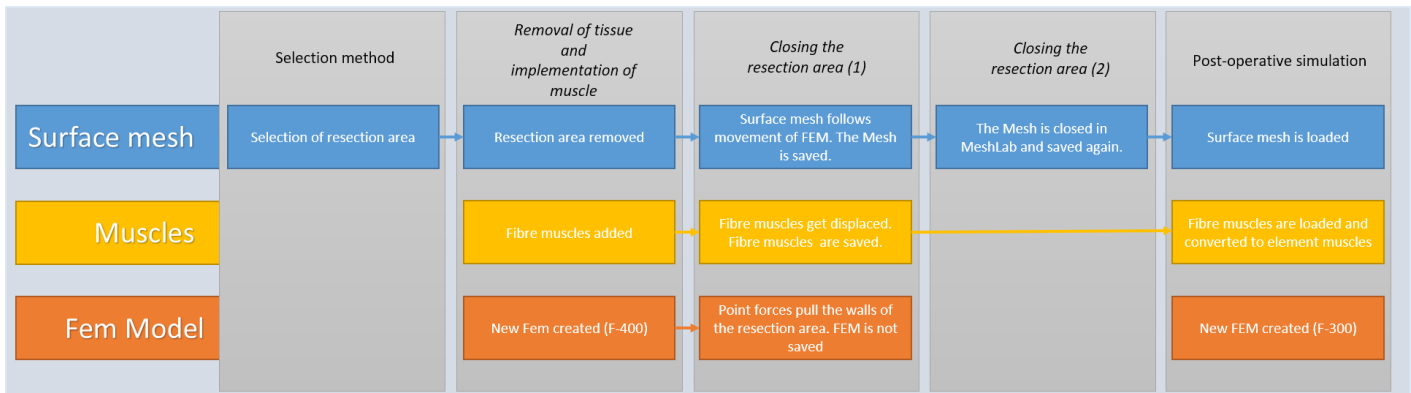


Figure 8: Flow chart to illustrate which parts of the model are involved in which part of the process.

a criterion is needed to come to a single solution. In this case, a “cost function” is used. This means, in this specific case, that the muscle combination with the lowest combined muscle excitations has to be found. More information details can be found in Appendix E.

2.6 Selection method

Selecting the resection area is the first step of virtual surgery. This only involves the surface mesh (see Figure 8). The primary goal of the selection method is to select the 3D resection area in the most user friendly way. This is difficult because this area has to be 3D. The use of 2D slices to draw the selection area where evaluated but were considered to be too time consuming. More futuristic approaches using virtual reality and a 3D cutting tool would be difficult to get. The best option seemed to be a point and click approach directly on the virtual model. The basic idea is that a selection area will be created by designating corner points of this area. With each click the selection area will be expanded with one corner point. The selection area is automatically closed by connecting the first and last corner point, and will be updated with each mouse click (Figure 9). The only condition is that the corner points are selected in the right order.

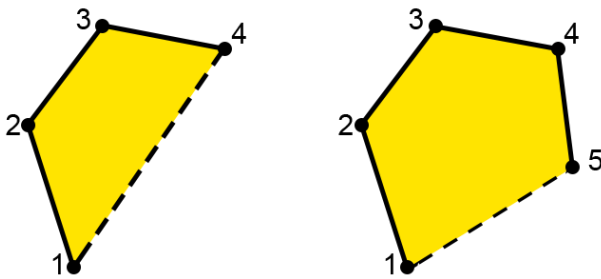


Figure 9: Principle of the selection method in 2D. The numbers refer to mouse-clicks.

However, Figure 9 is a 2D drawing and the tongue model is 3D. The interface of ArtiSynth is a 2D representation of a 3D object, in this case the tongue model. The user is looking at the tongue model from a certain angle. This is called the camera angle. When the user clicks at a location on the 2D screen a ray is cast at that point with the same angle as the camera. The objects that this ray encounters with each mouse click are the faces from the surface mesh (see section 2.2.1). After clicking, the faces will

be flagged as “selected”. For the selection method not every face that the ray encounters is a valid option for selection. To prevent the selection of faces on the opposite side of the tongue model the standard selection method in ArtiSynth had to be changed. Only the faces that are closest to the camera are selected. The centroid (midpoint of the face) of the faces will act as “corner point” for the drawing method. When more than two faces are selected it is possible to create an area as presented in Figure 9. Because the user must be able to turn the camera while selecting, ray-casting cannot be used to create the selection area (yellow area in Figure 9). Instead a 3D nonvisible area (made visible in Figure 10) is constructed as the user is selecting points. This will be done as follows:

- After each mouse click on the model do :
- For each selected face (i) do:
- Calculate centroid.
 - $C_{up}(i)$ = A point 1 mm* above the centroids of each face, in the direction of the normal.
 - $C_{down}(i)$ = A point 1 mm* below the centroids of each face, in the opposite direction of the normal.
- For all selected faces:
- Calculate the mean centroid of all selected faces
 - M_{up} = A point 1 cm* above the mean centroid of all selected faces, in the direction of the normal.
 - M_{down} = A point 1 cm* below the mean centroid of all selected faces, in the opposite direction of the normal.
- For each selected face (i) do:
- Create vertices using $C_{up}(i)$, $C_{down}(i)$ and $C_{up}(i+1)$
 - Create vertices using $C_{up}(i+1)$, $C_{down}(i)$ and $C_{up}(i+1)$
 - Create vertices using $C_{up}(i) + C_{up}(i+1)$ and M_{up}
 - Create vertices using $C_{down}(i) + C_{down}(i+1)$ and M_{down}
 - Create last vertices using the i'th points and the first points.

*The number is not relevant, it has to be elevated above or beneath the selected faces.

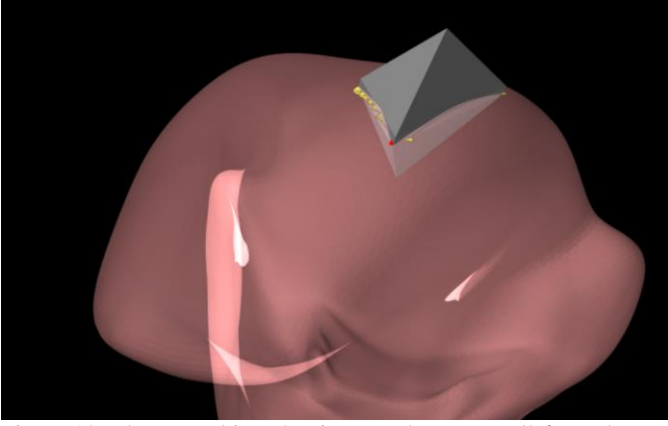


Figure 10: The grey object that is created to cover all faces that are selected.

The resulting (grey) 3D object is presented in Figure 10. Using a built-in function from ArtiSynth all faces within this object can be found. For every face on the surface mesh the centroid coordinates will be calculated. The function searches for the nearest face of the 3D object and determines if the normal of this plane is pointing away or towards the centroid of the specific face on the surface mesh. If the normal points towards the inspected centroid it is considered “outside the 3D object “. As long as there are no holes in the surface mesh this function works well. What’s left is an area of selected faces. After the selection of this area, the software not only needs to visualise the surface of the resection but also the depth and shape. When the user selects more than three points, the selected area has to be turned into a volumetric representation of the resection. To create a volumetric representation, the border of the selected area needs to be found. A built-in function can be used to identify all the edges of the border of the selected area. Border edges are only attached to one selected face instead of two. All vertices $\mathbf{P}_{v(i)}$ connected to these border edges will be saved. Using the vertices and their centre point \mathbf{P}_c (average of all vertices) the volumetric representation of the resection shown in Figure 11 is made.

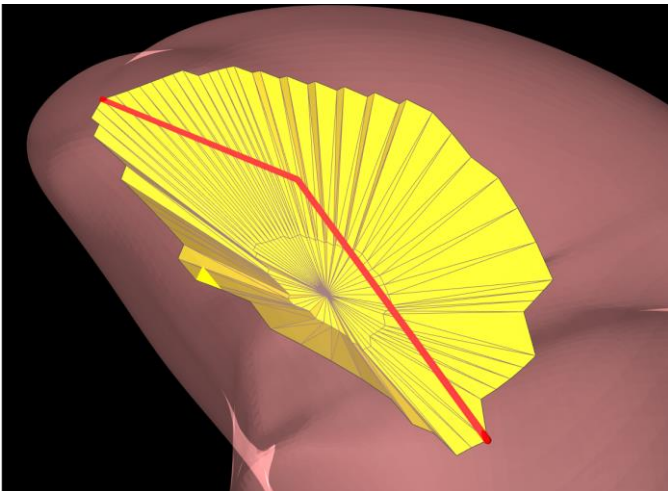


Figure 11: volumetric representation of the resection.

For now we are ignoring the red line. All the structures originating from the border vertices converge to the centre point. In between the vertices and the centre points are also newly created points: The halfway point ($\mathbf{P}_{hw(i)}$). These points can be dynamically adjusted in 2 directions: in the direction of the normal (\mathbf{n}) and perpendicular to the normal of the surface area (Figure 12).

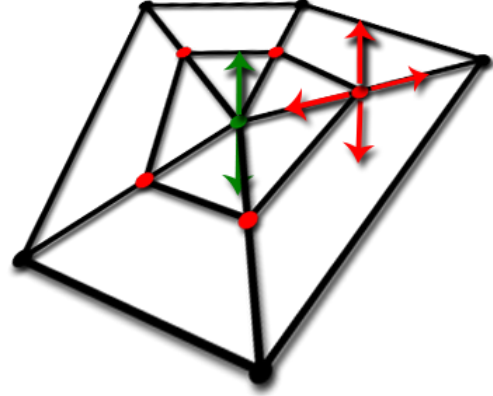


Figure 12: A topdown view of the volumetric representation of a virtual resection. Green: center point. Can only move in the direction of the normal. Red: half waypoints. Can move in the direction of the normal and in the direction of the centre point.

For this last adjustment the adjusted distance can be proportional to the shape of the resection or the absolute distance (Figure 13). This option, called adaptive shape, can be set on or off in the control panel (Figure 14). The centre point (\mathbf{P}_c) can only move in the direction of the normal and only relative to $\mathbf{P}_{hw(i)}$. First the centre point \mathbf{P}_c and the deep centre point \mathbf{P}_{dc} will be calculated:

$$\mathbf{P}_{dc} = (D_{hw} * \mathbf{n}) + \mathbf{C} \quad (6)$$

$$\mathbf{P}_c = \left(\left(\frac{D_{hw}}{2} * D_c \right) * \mathbf{n} \right) + \mathbf{C} \quad (7)$$

With D_{hw} = depth of halfway points (adjusted with slider on the control panel), D_c = depth of centre point (adjust with slider), \mathbf{n} = normal, \mathbf{C} = centroid of selected vertices.

For i = border vertices:

$$\mathbf{P}_{hw(i)}^* = (\mathbf{P}_{v(i)} + \mathbf{P}_{dc}) / 2 \quad (8)$$

Calculate directional vector $\mathbf{V}_{xyz(i)}$ from \mathbf{P}_c to $\mathbf{P}_{hw(i)}^*$

Calculate distance $V_{d(i)}$ between \mathbf{P}_c and $\mathbf{P}_{hw(i)}^*$

If adapt shape = true:

$$\mathbf{P}_{hw(i)} = \mathbf{P}_c + (\mathbf{V}_{xyz(i)} * (D_{CF} * V_{d(i)})) \quad (9)$$

If adapt shape = false:

$$\mathbf{P}_{hw(i)} = \mathbf{P}_c + (\mathbf{V}_{xyz(i)} * D_{CF}) \quad (10)$$

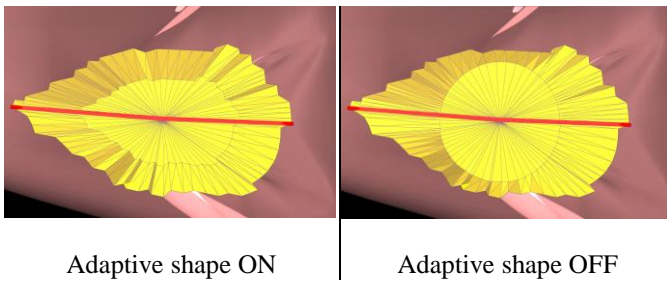


Figure 13: Sample of a volumetric representation of the resection to show the difference with and without the adapted shape method.

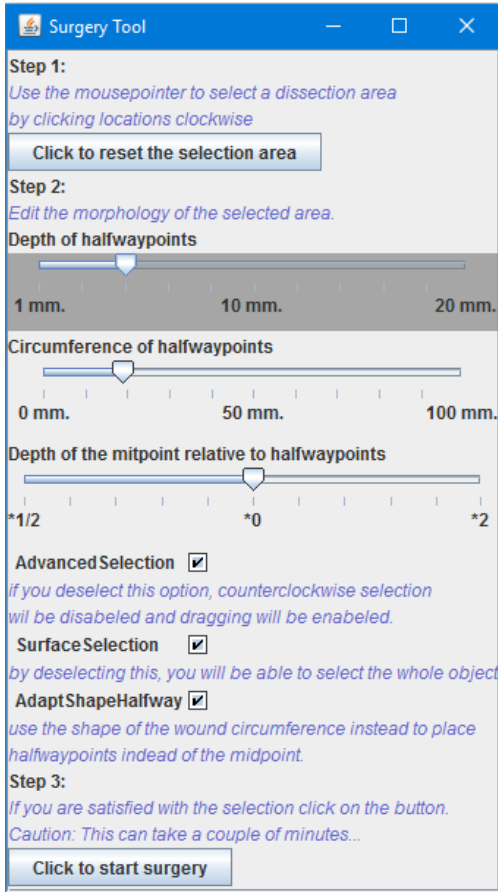


Figure 14: Control panel for surgery tool.

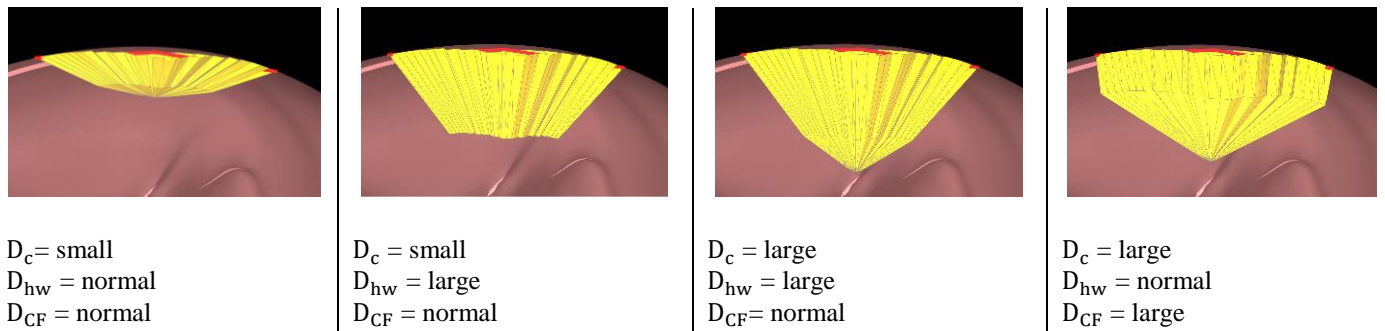


Figure 15: Different values for D_c , D_{hw} and D_{CF} are used to change the shape of the selection area.

P_{dc} will only be used to calculate $P_{hw(i)}$ which is the precursor of $P_{hw(i)}$ and will only be used to calculate $V_{xyz(i)}$ and $V_{d(i)}$. This step is essential to create the cone-like shapes shown in Figure 15. D_{CF} is the distance from the centre point to the halfway points. D_{CF} , D_{mp} , and D_c can all be changed with sliders on the control panel (see Figure 14).

This method appeared to be the most flexible and versatile way to select the location for a resection. The main advantage is that it cannot only create a hole but also an almost clear cut. By using the sliders on the control panel almost every shape can be created. Each time the input of a slider changes the method will instantly refresh the volumetric representation so that the user gets real time feedback.

2.7 Removal of tissue and implementation of muscle

At this moment the model consists of a surface mesh, a selected area on the surface mesh and a volumetric representation of the resection (see Figure 8). Vertices from the surface mesh corresponding with the vertices of the volumetric representation are also known. All corresponding faces and vertices from the selected area on the surface mesh except the ones on the edge will be deleted. By merging the corresponding vertices of the volumetric representation and the rest of the surface mesh the perioperative surface mesh is created. Using the same technique for constructing a FEM model as explained in “the new model” a new FEM is generated according to the new shape of the surface mesh. Using the coordinates of the muscle fibres from the initial model in ArtiSynth, muscles fibres can be placed inside the new FEM model (Figure 4). Muscles will only be placed if they are inside the mesh, so they will not be placed inside the resection. As will be explained in section 2.9, these fibres are not sufficient for the simulation of muscle contraction in the new model. They are, however, useful to transfer information about the changed muscle morphology due to the closing of the resection.

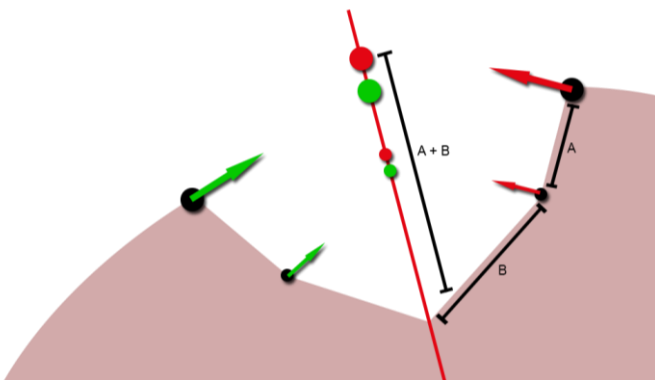


Figure 16: Illustration of the mechanism behind suturing of the model. Point forces are attached to vertices (black dots). These point forces are pulling the vertices towards the aim on the red plane.

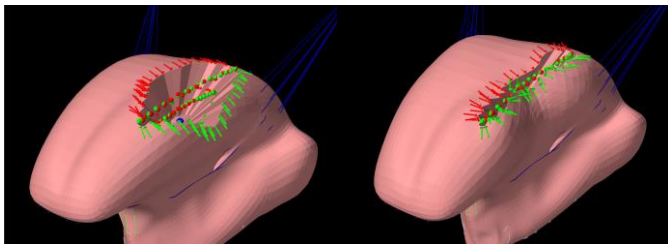


Figure 17: Visual representation of suturing with the surgery tool.

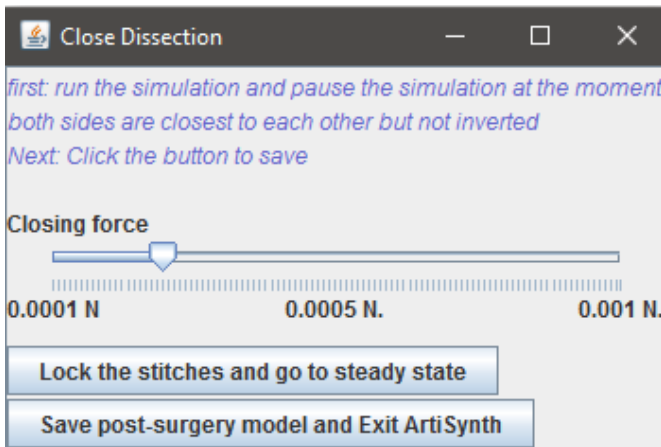


Figure 18: With the slider on the control panel the force that is generated in the point forces can be altered.

2.8 Closing the resection area

The main reason for splitting the surface mesh and the FEM model was the ability to implement the suturing of the resection. The most obvious way to close the wound would be to steer opposite points on the edge, on either side of the resection, towards each other. This is done using a point force; a force on a certain point in the FEM model. Because of the flexible way the volumetric representation of the resection is selected it is not known how many edge points there are, where they are located, and how they are ordered. It is therefore not always possible to detect opposite edge points. Instead, suturing will be simulated using point forces on the edge of the resection that move towards a (red) plane that is a cross section over the

largest diameter in the resection (Figure 16). The red line, visible in Figure 11, represents the future suture line, and thus the location of the plane. There is a hinge structure halfway the plane to deal with more complex shapes. For each edge point on either side of the plane the projection, and thus target point, on the plane is calculated. The target point on the plane will then be corrected for the distance between the edge point and the centre point of the resection ($A + B$ in Figure 16). This target point on the plane will be their target for the corresponding edge point. As can be seen in Figure 16 this method ensures that there will be as less as possible airspace left in the resection area. The target point on the plane will be levelled with the height of the near target points from the opposite sides (red and green points). In this way, when the resection is closed the opposite sides will be aligned.

When the simulation is started the edge point will slowly move towards their corresponding target point on the plane (see Figure 17). The forces will automatically be lowered exponentially when an edge point reaches their target point on the plane. Using a slider the user can adjust the global force manually (see Figure 18). As individual point forces will be lowered individually, increasing global force will have more effect on edge points with a larger distance from their target. A slider is also needed because different types of resections require different forces in order to close properly.

The drawback of using a plane is that the edge points of the resection (and thus other tongue tissue) are pulled towards a position on a plane that is not necessarily the “rest state” of the sutured tissue. Without dealing with this, the tissue could be pulled to an unnatural position. The last step ensures that the tongue tissue will move to a natural position. When both sides of the resection are close enough the user can “lock” the stitches so that edge points that are close to each other are fixed. The length of these stitches are fixed but the endpoints still have 3 degrees of freedom. When the forces are removed the tongue will return to a steady state where the stresses on the stitch are equally distributed.

At this moment, the FEM model, the surface mesh, and muscle fibres are changed in shape. There is no method available to fix both resection sides in the FEM model without distorting the whole FEM. Therefore, the FEM is removed and only the postoperative muscle locations and the surface mesh are saved (Figure 8). Using this mesh a new FEM structure can be created later the same way as described in section 2.4. Also the location of the resection will be saved to determine the volumetric area in which scar tissue is present later on. Using MeshLab the remaining hole in the mesh is closed.

2.9 Motion simulation

Using the method described in section 2.4 a new FEM structure is created from the postoperative surface mesh and muscle fibres. The muscle fibres, however, will not be used to act as actual muscles because of the following: In the initial model the two endpoints of muscle fibres are attached to nodes. This is convenient as an endpoint force will also be the force on that FEM-node. However, because of the new way in which the

FEM model is generated, muscle fibre endpoints are not located on the same spots as nodes anymore. The simulation would still work as the forces would be distributed automatically over the nearest nodes at an endpoint. The movement however would be unnatural. Elements that are in between elements containing a muscle fibre would get squeezed and are not actively involved in muscle contraction. This is not realistic and therefore not desirable. To overcome this problem a method is used to convert the fibre muscles to element muscles. Elements muscles can squeeze themselves and thus act as muscle parts. Elements have different mechanical properties which are described in section 2.5.3. Information about the position and direction of fibre muscles is used to convert normal elements to muscle elements. Elements that are within a diameter of four millimetre around a certain fibre are converted to element muscles with the same properties. A diameter of four millimetre ensures that most element muscle volumes are comparable with the FEM-muscle version of the initial tongue model (see section 2.3). The muscle forces in the element muscles now have the same direction as the nearby fibre muscles.

Using the information about the location of the resection, fibrosis (scar tissue) is added to the model. Not much is known about the exact extent of the fibrosis and the change in tissue properties of this location. Therefore a method, comparable with stiffening of tissue as part of the free-flap reconstruction approach in Buchaillard (2007)²², is used. Different amounts of stiffness will be used to simulate the stiffening at the former resection location (section 2.11). Also the volume in which the stiffness occurs will be varied in size to inspect the effects.

2.10 Validation by comparison with the initial model

First the parameters of the initial model will be compared with the new model. Parameters include: volume of the mesh, volume of the FEM model, number of elements and volume of individual muscle bundles. To compare the motion characteristics of the new model the displacement of the tip of the tongue, after an excitation of 0.3 (1 is maximum contraction) for each muscle, will be compared with the initial model. For this comparison the new model with size factor 200, 300 and 400 will be used.

2.11 Validation using patient cases

The initial model cannot be considered as the gold standard because it has never been validated using a patient study. So even more important than the comparison with the initial model will be the simulation of real patient cases. Therefore, pre and postoperative motion data from patients included in the ongoing study of van Dijk et al.²⁴ will be used. Using the surgery tool the surgical resections of three patients are imitated. This is done on the basis of pre and postoperative drawings of the surgeon.

2.11.1 Range of Motion measurement

In the study of van Dijk et al.²⁴ a validated method using 3D camera is used to measure the range of motion pre and postoperative¹⁵. Range of Motion (ROM) is expressed in the Euclidean distance between the tooth gap of the front teeth

(interdental papilla) and the tongue during a manoeuvre. These manoeuvres are: protrusion, left, right, elevation and depression.

Inclusion criteria:

Subjects (ages ranging from 18 to 90 years) undergoing partial glossectomy.

Exclusion criteria:

- Patients that are not able to fill in questionnaires
- Palliative treatment
- History of oral cancer treatment
- Radiotherapy on tongue surface

The 3D camera system consists of 3 camera's fixed in an angle of 20 degrees with a distance of 15 cm to each other. The cameras are then calibrated using an object consisting of 27 beads that are arranged on a 3x3x3 orthogonal grid¹⁵. For the information on tongue position reference points are placed on the tongue, the tip of the nose, between the eyes and 2 on the midline of the eyes (see Figure 19 and Figure 20).

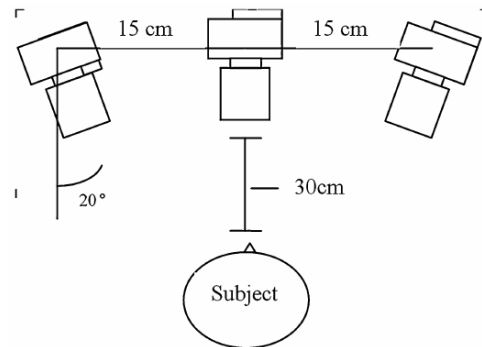


Figure 19: Illustration of camera setup used during the ROM measurements.

The first step in the offline analysis is the calibration of the interdental papilla with the markers on the face. This is because the distances will be expressed in the distance between tongue tip and interdental papilla. In the frames where maximal tongue excursion is achieved all markers and the tongue tip will be manually selected for all cameras (Figure 20). Using this information the 3D coordinates of these points can be calculated. The root mean square error of this operation is 0.73 mm.¹⁵ Interrater variability for both authors showed an interclass correlation (ICC) of 0.99 (95% CI 0.99-0.99 / CI 0.98 -0.99) and an intrarater variability of 0.95 (15% C I 0.93-0.97). The test-retest variability was 0.93(95% CI 0.89-0.93)¹⁵. This study is explained in more detail in Appendix F.

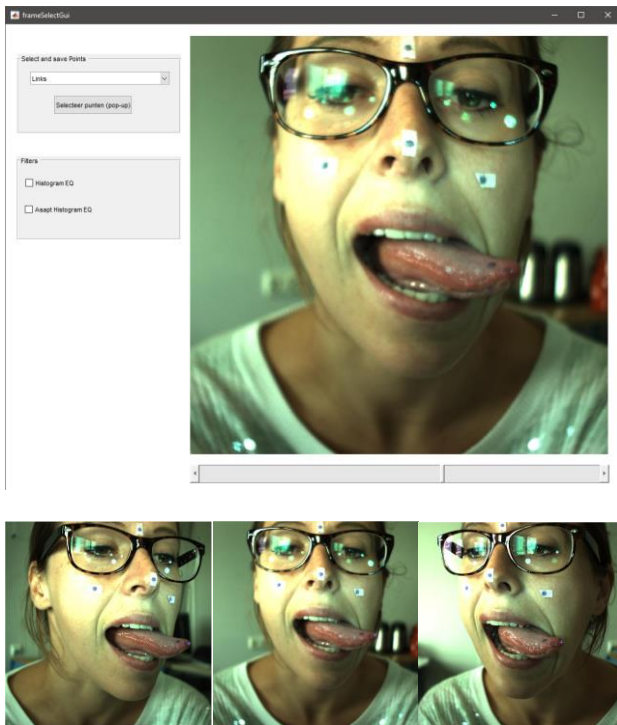


Figure 20: Upper image: a Matlab user interface used to select the reference points on the face and tongue. Lower images: The same image from 3 different camera's.

2.11.2 Forward simulation

Using inverse modelling the levels of muscle excitations that are needed for the manoeuvres: protrusion, left, right, elevation and depression are determined using a preoperative tongue model. These excitations are then used as input for the postoperative model of a specific patient. The difference between the initial position and the end position in a fixed direction will be the measure of tongue ROM in this research. A fixed direction means that the direction is fixed on the x, y or z axis. This will be compared to the difference between pre and postoperative motion of the three patients. To simulate the effect of scar tissue (or fibrosis), the tissue properties in the resection will be changed. Because the range of change is not known, different configurations will be used:

- no fibrosis
- 12x stiffness, 7 diameter around the initial wound
- 12x stiffness, 14 diameter around the initial wound
- 14x stiffness, 7 diameter around the initial wound

An increase in stiffness is defined as both c_{10} and c_{20} (see section 2.5.1) multiplied x times. These multiplication factors are chosen because “12x stiffness with 7 diameter” gave motion impairment percentages comparable to the ROM measurements of real patients. Other multiplication factors and diameters are omitted for the sake of clarity. This is decided on the basis of manual inspection of ROM measurements and simulations with the biomechanical model. No training set has been used to find the combination that is closest to the ROM measurements.

2.11.3 Inverse simulation

When the human body is exposed to a new situation, the body will try to adapt by compensating. With or without the help of a speech pathologist the patient can train himself to use other muscles to get (nearly) the same movements. This is, however, limited to what is possible with the new postoperative anatomy of the tongue. Using inverse modelling, postoperative models will be forced to find a way to perform a certain manoeuvre. These movements will also be compared with the real patient cases. Only 12x stiffness with a diameter of 7 diameter around the wound is used. In forward modelling this is the setting that is most comparable to the ROM measurements. Additional configurations of the inverse simulation have no added value for this stage of research.

2.11.4 Video inspection

In the results and discussion it will become clear that the Euclidean distance from the ROM measurement is not the best method to validate the biomechanical model. The video inspection is added to compare the forward and inverse simulation directly with the visual inspection of the recorded video. This visual inspection is done solely by the author of this report to give a qualitative measure to compare the biomechanical model with.

3. RESULTS

3.1 Initial model versus new model.

Table 2 shows a comparison of basic properties between the initial model and the new model using a size factor of 200, 300 and 400. The nodes and elements after elimination are showing the amount of nodes and elements left after deleting those which were not inside the surface mesh. It is obvious that the model with size factor 200 has an amount of elements that equals the initial model. Therefore this model simulates movement very quick. However it can be noted that the volume of this FEM model is larger in comparison to the models with size factor 300 and 400. The higher the size factor of the FEM model (and thus amount of elements) the more comparable the volume is to the volume of the surface mesh. There is no volume difference for the surface mesh and FEM model of the initial model as the surface mesh is of the same shape as the FEM model.

Table 2: Volumes of the FEM Models and Surface meshes and the amount of element for and after elimination.

	Initial Model	F 200 (15x14x12)	F 300 (23x20x18)	F 400 (31x36x24)
Nodes at start:	947	2912	9576	21600
Elements at start:	739	2340	8280	19344
Nodes after elimination:		1654	4776	9862
Elements after elimination:		1186	3735	8096
Volume of Mesh in cm³	102.29	108.47	108.47	108.47
Volume of FEM in cm³	102.29	157.85	143.09	133.06

Table 3 shows the volume of each muscle in the initial model and the new model with size factor 200, 300 and 400. The initial model, in this case, is the FEM muscle version of the initial model. This is because the fibre muscle model uses fibres, and fibres do not have a volume. The FEM muscle version of the initial model is made in such a way that it closely resembles the forces from the initial fibre model.

In order to get comparable motions in the new model, muscles have to match the volume of the initial model almost completely. With fibres converted to elements with a diameter of four millimetre around the fibre (see section 2.7) high volume muscles are matched almost completely. But even after diminishing the diameter, the SL and HG muscles remained about four times larger in comparison to the initial model.

Table 3: Volume of muscle bundles in cm³ and in % of total volume. Displayed are the initial tongue model and the factor 200, 300 and 400 version of the new model.

	Initial model		factor 200		factor 300		factor 400	
GGP_L	9.20	9%	15.53	12%	15.48	11%	15.00	11%
GGP_R	9.20	9%	15.16	11%	15.40	11%	14.48	11%
GGM_L	1.8	2%	5.51	4%	6.14	4%	6.06	5%
GGM_R	1.8	2%	5.39	4%	6.14	4%	5.89	4%
GGA_L	2.25	2%	6.01	5%	6.14	4%	6.15	5%
GGA_R	2.25	2%	5.89	4%	5.87	4%	5.96	4%
GH_L	1.96	2%	5.39	4%	4.73	3%	4.52	3%
GH_R	1.96	2%	5.01	4%	4.69	3%	4.39	3%
MH_L	3.34	3%	10.52	8%	9.53	7%	8.37	6%
MH_R	3.34	3%	10.40	8%	9.49	7%	8.32	6%
HG_L	2.97	3%	14.28	11%	15.06	11%	14.62	11%
HG_R	2.97	3%	13.78	10%	15.18	11%	14.39	11%
VER_L	16.59	16%	20.42	15%	21.20	15%	21.46	16%
VER_R	16.59	16%	20.55	15%	21.50	15%	21.43	16%
TRA_L	18.22	18%	26.43	20%	26.65	19%	26.64	20%
TRA_R	18.22	18%	26.06	20%	26.58	19%	26.15	20%
IL_L	2.25	2%	11.78	9%	11.52	8%	11.07	8%
IL_R	2.25	2%	11.78	9%	11.48	8%	11.05	8%
STY_R	2.48	2%	0.00	0%	0.00	0%	0.00	0%
STY_L	2.48	2%	0.00	0%	0.00	0%	0.00	0%
SL_R	8.50*	8%	39.71	30%	34.39	24%	32.94	25%
SL_L	8.50*	8%	39.46	30%	34.28	24%	32.43	24%

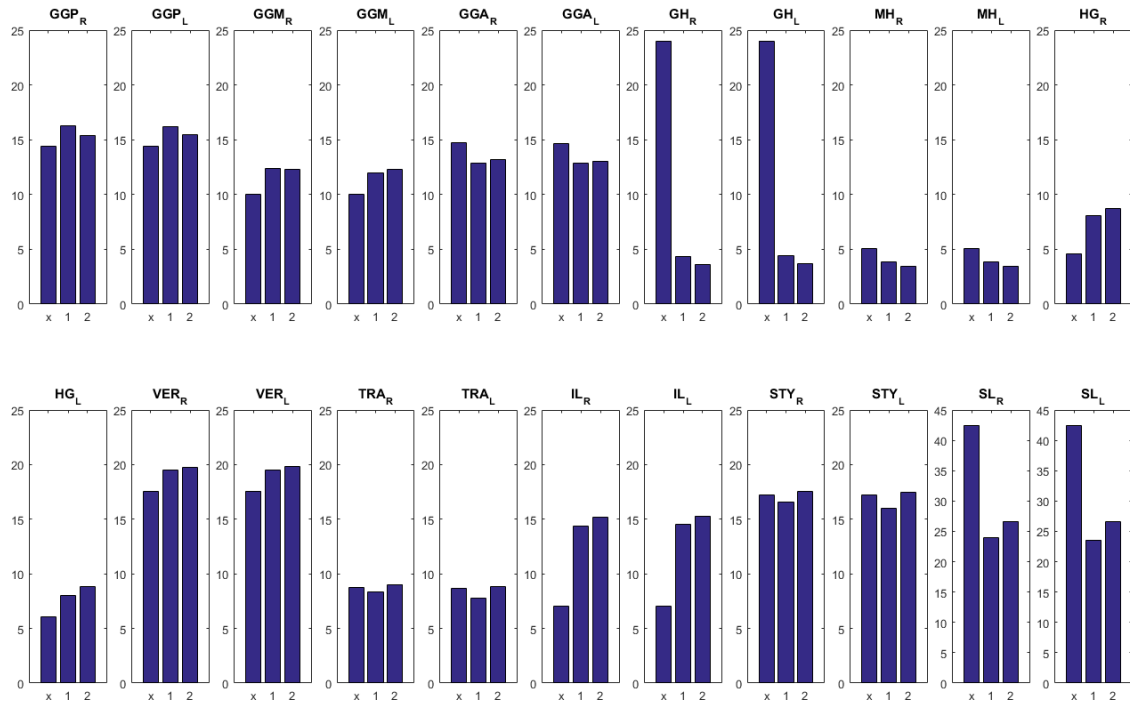


Figure 21: Euclidean distance in mm. between the tongue tip and the interdental papilla after an excitation gain of 0.3 on a certain muscle. x is the original model, 1 is the new model with size factor 200, 2 is the new model with size factor 300. The Y axis of the SL muscle is of another range than the other muscles.

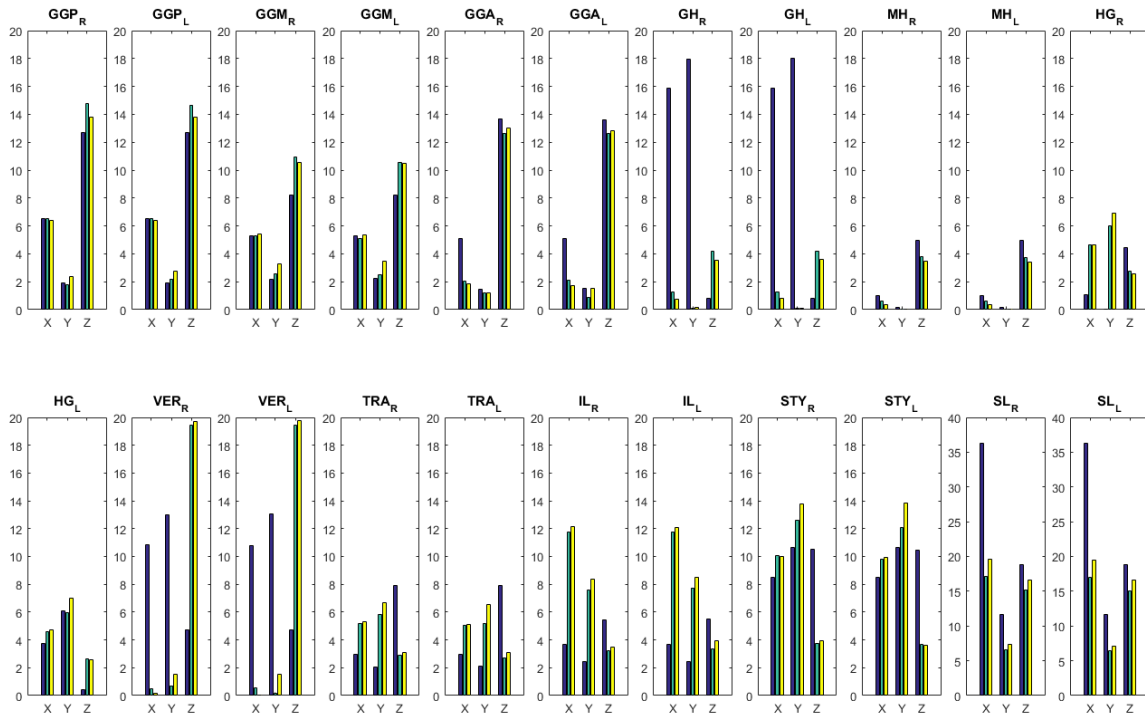


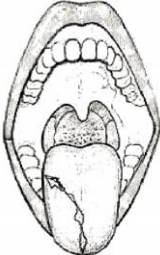
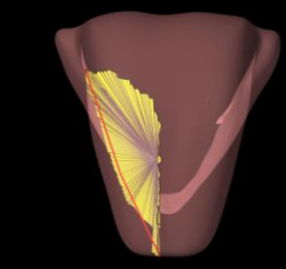
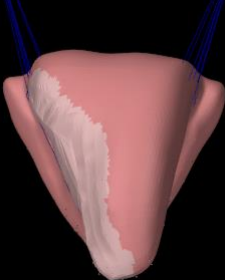
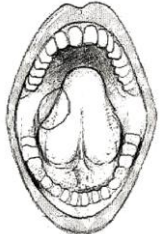
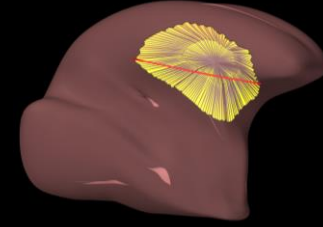
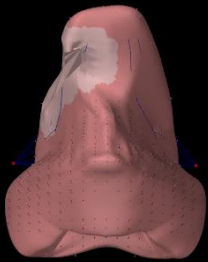
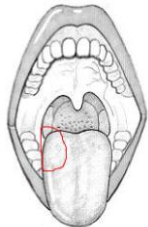
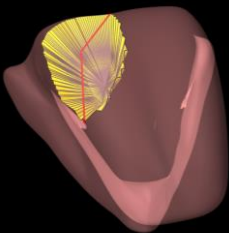
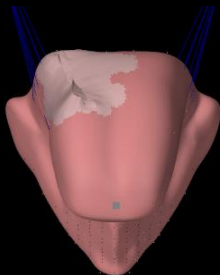
Figure 22: Coordinates of the tonguetip in mm. after an excitation gain of 0.3 on a certain muscle. Blue is the original model, Green is the new model with size factor 200, Yellow is the new model with size factor 300.

The comparison in Figure 21 shows the differences in Euclidean distance after an excitation of 0.3 on a single muscle. The purpose of this and the next graph is to compare the reaction of the new and initial model after the excitation of a muscle bundle. From the new model only size factor 200 and 300 are used. A size factor of 400 takes up to much time for a single simulation and is therefore not used for simulation of manoeuvres (only during virtual surgery). The smallest differences can be seen between the factor 200 model (Number 1) and the factor 300 model (Number 2), which are consistent in all muscle bundles. It seems that the model with size factor 300 model is better comparable to the initial model than the factor 200 model. The movement of the GH as well as in the SL muscle are significantly higher in the initial model, while those muscles are much more voluminous in the new models.

different models appeared to be almost the same when looking at the Euclidean distance, this graph highlights another aspect. The movement of the initial model after activation of the GG muscle seems to be almost the same as that of the new model. The GH from the initial model has a large movement in the Y direction in comparison with the new model. This same effect can be seen for the SL muscle in the X direction. The movements of the intrinsic muscles VER and TRA are noticeably different from the initial model, while the Euclidian distance is almost the same. Both the GH and VER show a large movement in Z direction in the new model and a large movement in X and Y direction in the old model. Generally, it can be seen that a small difference in Euclidean distance can still be a quite high actual position difference.

Figure 22 shows the same models and movements but now in 3D coordinates. The factor 200 model only received an excitation of 0.18 on the SL muscle because a gain of 0.3 caused inverted elements in this case. Although movements of the

Table 4 Postoperative drawings, selection area, postoperative model and stats of three models based on patient cases. The grey area on the postoperative model is the visual representation of scar tissue.

	Selection of resection area	Postoperative model	Model characteristics
Patient 1 Post-operative drawing 			Volume difference after surgery: In Mesh: 5.77 mm ³ (5% of total volume) In FEM: 7.21 mm ³ (5% of total volume)
Patient 2 Preoperative drawing 			Volume difference after surgery: In Mesh: 1.57 mm ³ (1% of total volume) In FEM: 1.61 mm ³ (1% of total volume)
Patient 3 Post-operative drawing 			Volume difference after surgery: In Mesh: 2.08 mm ³ (2% of total volume) In FEM: 1.91 mm ³ (1% of total volume)

3.2 Patient cases

Three patient cases were included for the validation process. For each patient the pre- and postoperative drawings, the created virtual resections and model characteristics can be found in Table 4. Forward simulations, inverse simulations and the ROM measurements are summarised in one table for each patient (table 5-7). The patient characteristics and video inspection are explained in plain text.

Table 5: Percentages of the differences between the pre and postsurgical final position of the tip of tongue in a certain direction after performing a manoeuvre.

Patient 1: pre- versus postsurgery					
Forward simulation					
Distance in direction of manoeuvre					
	protrusion	contralateral	ipsilateral	elevation	depression
no fibroses	2%	5%	6%	-5%	11%
12x stiff. 7 diameter	16%	12%	13%	16%	29%
12x stiff. 14 diameter	33%	33%	29%	42%	53%
14x stiff. 7 diameter	21%	17%	36%	24%	35%
Inverse simulation					
Distance in direction of manoeuvre					
	protrusion	contralateral	ipsilateral	elevation	depression
12x stiff. 7 diameter	16%	6%	4%	0%	24%
Patient ROM measurement					
Euclidean distance					
	protrusion	contralateral	ipsilateral	elevation	depression
	49%	-5%	10%	38%	30%

Patient 1 characteristics

The first patient (57 y/o) was treated for an T1 Squamous cell carcinoma ventral right with unknown amount of affected lymph nodes and zero metastasis (T1NxM0). The diameter of the tumour is 1.8 cm. Because of deep tumour strands there was an additional resection of 4 mm. of the deep edge of the initial resection. The resection volume is 26 mm³. As can be seen on the postoperative drawing in Table 4 a large part of the right anterior and lateral part of the tongue was removed during surgery. The postoperative model shows a tongue, missing many right superficial muscles and a large volume with scar tissue where the wound is closed.

Video Inspection

Postoperative, there is a clear deviation to the ipsilateral side while protruding. The patient cannot elevate the tongue anymore. Before surgery this was about 1 cm. While pointing the tonguetip to the ipsilateral side the reach is about 1 cm less. The largest impairment can be seen while depressing the tongue. Then the range is about 4 cm less.

Patient ROM measurement

Presented in Table 5 are the percentage differences in Euclidian distance of a manoeuvre pre- and postoperative. The patient ROM measurement gives a largely comparable result with the video inspection. But as this is the Euclidian distance, the

protrusion could be under- or overestimated because the tongue was moving to the ipsilateral side too. The impairment while depressing the tongue seemed larger on the video than in the ROM measurements.

Forward simulation

Presented in Table 5 are the percentage difference between the movement in a given direction (not the Euclidian distance) pre and postoperative. With no fibrosis there is almost no change in pre- and postoperative movement. With 12x increased tissue stiffness over a diameter of 7mm around the former resection area the differences become larger. As the exact postoperative properties are unknown, the best setting for fibrosis remains difficult to estimate. Comparable with the video inspection and the patient ROM measurements is that ipsilateral deviation is larger than the contralateral deviation. Also the deviation in depression, which is larger than most other impairments, is comparable with the video inspection. The impairment while protruding is larger in the ROM measurement than in the forward simulation. However it can be seen that in the video inspection the tongue moved to the ipsilateral side while protruding and thus probably gives a overestimation.

Inverse simulation

In the inverse simulation the same impairment can be seen while protruding, but the other impairments are certainly less. The impairment to the ipsilateral side is slightly larger in this case which is not in line with the forward simulation and ROM measurements. Also elevation shows no impairment at all versus 16% in the comparable forward simulation. There are apparently other muscles in this model that can be used to move the tip of the tongue to the same position.

Table 6: percentages of the differences between the pre and postsurgical final position of the tip of tongue in a certain direction after performing a manoeuvre.

Patient 2: pre- versus postsurgery					
Forward simulation					
Distance in direction of manoeuvre					
	protrusion	contralateral	ipsilateral	elevation	depression
no fibroses	4%	-3%	4%	-6%	2%
12x stiff. 7 diameter	15%	14%	11%	2%	13%
12x stiff. 14 diameter	31%	34%	30%	28%	42%
14x stiff. 7 diameter	18%	21%	14%	5%	17%
Inverse simulation					
Distance in direction of manoeuvre					
	protrusion	contralateral	ipsilateral	elevation	depression
12x stiff. 7 diameter	18%	10%	7%	-1%	14%
Patient ROM measurement					
Euclidean distance					
	protrusion	contralateral	ipsilateral	elevation	depression
	-43%	19%	-7%	-15%	20%

Patient 2 characteristics

The second patient (67 y/o) was treated for an T2N0M0 squamous cell carcinoma on the right lateral tongue edge. There was no peri- or postoperative drawing available, so the virtual surgery is based on a preoperative drawing of the tumour location and the written report. The exact dimensions of the resection are not known. The resection volume is 16 mm³.

Video inspection

After surgery there is a small decline of about 5 mm. when protruding and a deviation to the ipsilateral side. When the patients tries to move to the ipsilateral side the tongue depresses almost 40 degrees. Movement to the contralateral side is 1 cm. less in the postoperative situation. Elevation of the tongue is almost not possible preoperatively and looks slightly worse after surgery.

Patient ROM measurement

The patient shows an improvement of 43% in Euclidean distance when protruding. This was clearly not the case in the video inspection. Instead, the tongue pointed into a different direction in the postoperative video. There is also a 7% improvement when moving the tongue to the ipsilateral side. Also this is questionable as video inspection shows that the tongue depresses instead of moving to the ipsilateral side. Postoperatively the patient cannot elevate the tongue above her front teeth so an improvement of 15% is also unlikely.

Forward simulation

Looking at the forward simulation, there are no real outliers. The decline in motion is mostly the same using all settings. With a fibroses diameter other than 14 mm the decline in elevation is almost non existing. This is comparable to the video inspection showing no outliers in pre and postoperative differences.

Table 7: percetages of the differences between the pre and postsurgical final position of the tip of tongue in a certain direction after performing a manoeuvre.

Patient 3: pre- versus postsurgery					
Forward simulation					
Distance in direction of manoeuvre					
	protrusion	contralateral	ipsilateral	elevation	depression
no fibroses	0%	6%	5%	-5%	10%
12x stiff. 7 diameter	2%	10%	4%	2%	15%
12x stiff. 14 diameter	11%	22%	13%	13%	30%
14x stiff. 7 diameter	3%	11%	5%	4%	17%
Inverse simulation					
Distance in direction of manoeuvre					
	protrusion	contralateral	ipsilateral	elevation	depression
12x stiff. 7 diameter	3%	11%	5%	-6%	16%
Patient ROM measurement					
Euclidean distance					
	protrusion	contralateral	ipsilateral	elevation	depression
	-32%	30%	10%	30%	7%

Inverse simulation

The results of the inverse simulation are comparable with the forward simulation. Overall there seems to be no improvement in motion capabilities by using other muscles to get the same movement.

Patient 3 characteristics

The third patient (56 y/o) was treated for a T1N0 squamous cell carcinoma at the right tongue base. The ulcer had a diameter of 5 mm and a depth of 1.5 cm. The volume of the tumour is 13 mm³.

Video inspection

Protrusion is a little less far but not very different from the preoperative video. The motion to the contralateral side declines about 5 mm while the motion to the ipsilateral side remained the same. There is a huge elevation of the tongue pre and post-operatively and the depression did not change notably.

Patient ROM measurement

There are large changes in Euclidian distance in the ROM measurements while there are no large differences at video inspection. The only large difference at video inspection was a decline in motion to the contralateral side and a little decline while protruding. The decline in motion at the contralateral side is also visible in the ROM measurements but the improvement in protrusion is probably not realistic.

Forward simulation

In the forward simulation a decline in motion to the contralateral side is also visible in the “12x stiff 7 diameter” simulation. Depression showed a significant change in motion during the simulation, while this was not noticed at video inspection. The other differences are small, which is comparable to the video inspection

Inverse simulation

There is no noticeable difference between forward and inverse simulation other than that elevation could be improved somewhat. Elevation is even better than in the preoperative model.

3.3 Patient comparison

In the ROM measurement, video inspection and biomechanical model the largest impairment can be seen in patient 1. The resection volume of patient 1 is a much larger than those of the other patients. The resection volumes of patient 2 and 3 as well as the motion impairments were more comparable. In all three patients, the biomechanical model does not show the same proportions in impairment as the ROM measurements. However, it appears that the biomechanical model is more comparable to the video inspection than to the ROM measurement. By comparing the patient measurements with the video we see that the impairment for a motion to the contralateral side is larger than for a motion to the ipsilateral side. This is less noticeable in patient 1, who had undergone a resection at the anterior part of the tongue.

4. DISCUSSION

In this report, a method to perform virtual surgery on a biomechanical model was presented. An easy to use tool is created to select and shape a resection volume. Also a new way of creating a FEM model was presented. After suturing the virtual resection and adding scar tissue, the postoperative tongue of three patient was imitated. Results show that, although not all muscle volumes and forces are comparable with the initial model of Buchaillard (2009)²³, postoperative movements of the model show similar impairments as patients on the video recordings.

4.1 The model

The initial tongue model is based on an atlas of 10 patients and then morphed to one patient specific model to get a general representation of the tongue while maintaining the details of the tongue^{17,18,22,23}. The tongue was then transformed to a low resolution FEM model. The surface mesh used in this report is a smoothed version of the surface from this low resolution FEM model, and is therefore not a perfect resemblance of either an atlas or a personalised model of the tongue. As the postoperative movements of an atlas model cannot be validated, the next step would be to acquire a segmented FEM or surface mesh from patients included in the ROM measurement studies. This would also require personalised muscle configurations, which will be explained later in this discussion. Also closing of the hole in the mesh after surgery is visually far from perfect (Table 2). No better method was found to close this mesh, but it probably would not affect postoperative motion as the area is very small.

The method used in this report to separate the surface mesh and FEM model has never been used before. A FEM model that also represents the exact tongue shape, like the initial model, forces researches to work with low resolution handmade models. The only way to edit these kind of models is by altering tissue properties or by removing huge elements. Separating the surface mesh and the FEM model made it possible to easily edit detailed parts of the tongue and actually remove a part from the model. This on its turn made it possible to create virtual sutures to close the resection. This step is practical as most of the surgeons in the Netherlands use primary closure using suturing during a glossectomy instead of free-flap reconstruction¹⁴.

The method for creating the new model, however, is far from optimal. The FEM model consisting of cubic shaped elements is created according to the shape of the surface mesh. In order for this to work, the mesh needs to be completely enclosed in the fem model. Otherwise, muscles fibres are placed outside the FEM model. This happens often in case of the SL muscle, which is located on the top surface of the tongue. The problem which arises when enclosing the mesh in the FEM model is that the volume of the FEM model will be larger than the volume of the surface mesh. By increasing the amount of elements in the FEM model the surface will be matched more precise and the volume of the FEM model will be more comparable to the initial model. However it will still be almost 25% too large (Table 2). The increased weight is not a problem, as argued in the method section, but the resistance created by the amount of

tissue probably is. A better way to match the volume would be to only include elements that are for more than 50% within the surface model. But then again, a solution has to be found for the muscle fibres that are placed outside the FEM. It also remains questionable if enabling the placement of fibre muscles outside the FEM model, only for the purpose of creating element muscles around them, would give better movement of the tongue. The real solution would be a FEM morphing solution in which different shapes of elements are automatically created to match the surface mesh. As discussed in Appendix D, creating a perfect matching FEM model for every surface mesh is still a challenging topic.

Implementation of muscle bundles is one of the weaker parts of the new model. The bundles that are used are extracted from the initial model of Buchaillard²³. As mentioned earlier, this model consists of a limited amount of elements. Muscle fibres in this model are made to connect only to the nodes of those elements. The muscle fibres are therefore also of a low resolution and do not have a smooth curvature (Figure 4). These fibres are not directly used as actual muscles in the new model but as guidance for where the element muscles need to be generated. This method appeared to be a weakness for a couple of reasons: The diameter to indicate the extent of the area in which elements around the fibre are needed to be converted too muscle elements is never sufficient. When the diameter is too small there will be elements between fibres of the same muscle that are not converted to a muscle element. This is not realistic because every spot in a tongue is supposed to be muscle tissue. On the other hand, a large diameter can increase muscles to unrealistic volumes and can cause them to overlap too much. With the FEM model being larger than the surface mesh also elements outside the surface mesh will act as muscle. This is probably the case with the HG and SL muscle. These muscles are both on the surface and thus use all the redundant elements on the surface of the FEM model. On the other hand, even with a larger diameter there are still elements that are not converted to muscle, because these are not around the fibres on spots where fibres make a large angle (Figure 4). It is not entirely clear why the VER and TRA show such a different movement in comparison to the initial model in Figure 22. This is probably also due the lack of resolution in the original fibre muscle data. Localization of the element muscles and resolution of the muscles could be improved by using data from the FEM muscle version of the initial model. The difficulty was that an altered muscle morphology after suturing of the resection has to be transferred somehow to the new postsurgical model without saving the actual muscle elements. This however would be a time consuming effort, and a lot of the problems that exist with the muscles of the fibre model would still exist using this model. A more important reason to not use the element muscles from the initial model is that future personalised models would make use of fibres that are acquired using Diffusion Tensor Imaging (DTI). Great progress could be made by increasing the amount of muscle fibres and redefining the shape using these DTI images. This would be a better focus than improving the muscles from the initial model. In future perspectives, new ideas for the registration and implementation of muscle bundles are discussed.

The GH and SL muscle have large volumes in the new model in comparison to the initial model but induce a significantly smaller movement with an excitation gain of 0.3. The original fibres of these two muscles are on the surface of the tongue, and when activated they act as a kind of “lever” for upward movement. One reason for the smaller movement could be that due to the large volumes of the element muscles, excitation results in a squeezing movement instead of a “lever” movement. Another explanation is that the amount of force a fibre can generate at a gain of 1 is determined by a pre specified value, while the force of an element is determined by its volume. This pre-specified value is in no relation to the amount of fibres while the amount of elements have a direct relation to the amount of fibres.

The selection method to implement virtual surgery works well. It is possible to create most shapes used for resections with this simple tool. However, the shapes are not sleek. The virtual resection is created from faces on the surface mesh of the model. They are restricted because of the method used to create these virtual resection. More advanced programming could implement truly smooth areas that are created independent from the existing surface mesh. However, it can be argued that smooth shaping is not necessarily needed with these types of surgery, where the exact resection cannot be planned in detail. Creating 3D objects for the selection of faces on the surface is not the most straight forward and computational efficient method. But again, the final selection would not differ much if the method was faster or more efficient.

When looking at the postoperative volume differences something remarkable can be seen. The removed tissue volumes in the model are very small. One reason for this is that, as mentioned earlier, the FEM model extends beyond the surface mesh model. Therefore the resection volume in the actual FEM model is relatively smaller than in the surface mesh. But that is not the only reason. As can be seen, also the surface mesh nearly changes after virtual surgery. The problem is that when the resection is closed it cannot be closed entirely. There will always be a gap because of the restriction in movement of the FEM model. After surgery this gap is closed and fibrosis is added. Although this area has no active muscles anymore, it will still contribute to the postoperative volume.

4.2 Patient comparison.

Comparison of the biomechanical model with patients is difficult. Especially because techniques to measure functional impairment/motion of patients are still not well developed. The virtual resections were based on postoperative or preoperative drawings from the surgery. From the 10 patients currently included in the ongoing ROM study of van Dijk et al.²⁴, only 3 patients include one of these drawings. This is unfortunate, as a surgical resection cannot be simulated without a drawing of the area. But even with those 2D drawings the actual location and shape of the 3D area remains uncertain. Validation of the tumour resection volume in the virtual surgery model was also not possible because it is not a personalised model. Therefore volumes of the patients tongue are not comparable.

In the ROM measurements, positions of the tongue are registered in coordinates of the camera system. This means that when the head of the person is not perfectly aligned with the camera in the pre and postoperative recording the directions of the movements cannot be compared. It is also difficult, if not impossible, to correctly align all the coordinates of the video with those of the model. However, the Euclidian distance between the tooth gap of the person’s two front teeth and the top of the tongue can be calculated. This is the reason why the results of the biomechanical model are expressed in distances in a certain direction and results from the measurements are expressed in Euclidian distances. In essence, this Euclidian distance is not the ultimate measurement method as a totally different direction could still give a comparable Euclidian distance (as long as the distance is the same). Without inspecting the videos these results could give a distorted picture. In order to really compare directions, pre and postoperative in the future, the coordinate system needs to be calibrated with the head of the specific patient. Details will be discussed in future perspectives.

When trying to compare the ROM measurements to the movements of the biomechanical model, the opening of the jaw also needs to be implemented. While depressing and protruding the tongue, the jaw is opened at a certain angle. This also happens during other manoeuvres with the tongue. When tongue movements of the patient are simulated with the biomechanical model these angulations need to be taken into account. This is particularly important as the complete orientation of the tongue changes when the angle of the jaw changes. Other muscle combinations are used when the tongue is in a different position.

Considering these limitations, the results can be interpreted again. In patient 1 we see that the virtual model correctly predicts an impaired movement when depressing the tongue. There is not much impairment at the contralateral side. Patient 2 and 3 underwent resections at the back of the tongue and closer to the tongue base. These resections tend to have a more significant effect on contralateral movement. This is in line with literature that states that tumours closer to the tongue base result in more motion (and thus speech) impairment⁹. Overall postoperative movement of the model seems to be in line with the video inspection of the patient. On the contrary ROM measurement, in its current state, seems less suitable for validation of the virtual surgery model. Hopefully there are ways to acquire better coordinates from the video’s that are already made.

It is remarkable that in a model where so many assumptions are made, there is already a tendency to predicting the right postsurgical impairment. By taking away those assumptions and by personalising and improving the model it could be on its way to eventually predict the functional outcome of a partial glossectomy.

5. FUTURE PERSPECTIVE

5.1 *Personalised tongue mesh*

The mesh that was used for the tongue was a mesh that is based on an atlas of 10 patients and then morphed to one specific patient. The morphing is done because a mesh made of an atlas does not look like an actual tongue. This results in a general tongue model that is still personalised to an unknown person. It is not possible to validate a model in detail for postsurgical impairment when the preoperative model does not have the same shape and volume of the patient. The next step would be to create or adapt a segmentation method to segment the tongue shape and volume.

5.2 *Personalised muscle bundles*

Muscle orientation and strength, just like shape and volume, differs much between persons. To simulate postoperative motion in detail, the individual morphology of all tongue muscles is needed. Only then will the right muscles will be removed or displaced during virtual surgery. At this moment Diffusion Tensor Imaging (DTI) seems to be the right technique for this purpose. DTI is frequently used for the visualisation of neural axons in the human brain. It is a technique that uses the Brownian motion of water molecules to generate contrast in images. It is a method to visualise the diffusion processes in tissue. In fibre muscles as well as axons, diffusion is faster in the direction of the fibre. Because of this phenomenon it is possible to find the direction of the diffusion which makes it possible to visualise the muscle fibre directions³⁸. Ongoing research at the NKI, Academic Medical Center (AMC) and other institutes is focused on improving acquisition sequences to get clear muscle fibre directions from the tongue^{39,40}. This fibre data can be used instead of the low resolution fibre data of the initial model to create a truly personalised model.

5.3 *Stiffness & fibrosis*

Every person's skin is different and feels different, so are the tissue properties of the tongue. Researchers did not succeed to find the correct tissue properties for a moving tongue of a living person yet^{23,34}. The best effort for the initial model and the new model was to use both limited data from living and dead tissue²³. In addition to these difficulties, tissue properties also varies between persons. There are methods to measure stiffness with an MRI, but also other methods are being evaluated at the NKI and AMC. Imaging of soft tissue strain and elasticity using ultrasound seems to be a promising cost saving and accessible solution. For the prediction of postoperative impairment a personal preoperative biomechanical model is not enough. Many so far unknown tissue reactions are happening in the resection area and not much is known about the exact development in this region in terms of tissue properties. A next aim is therefore to find tissue properties and the extent of scar areas after surgery. As can be learned from the results of this report, scar tissue has a significantly influence on the postoperative mobility of the tongue and is therefore crucial for the functional outcome.

5.4 *Improved FEM structure*

The automated creation of the FEM structure for the new model was forced to be a structure consisting of cubic elements, since no method is available that can automatically create a FEM model consisting of a hexahedral mesh that is completely adapted to the shape of the surface mesh. Automatic mesh generation is only possible with tetrahedral elements, which cannot be used for the tongue model as they are prone to volumetric and shear locking. Details of this principle are explained in Appendix D. New techniques are being developed where mixed meshed are used to automatically create complex FEM shapes. Here tetrahedral elements are used for parts of the surface with a big curvature, but inside, the mesh is completely hexahedral⁴¹. This mixed mesh model showed no large differences to the original all hexahedral mesh. Using this kind of automatic meshing would be beneficial for the further development of the virtual surgery model.

5.5 *Techniques for measuring pre and postoperative tongue motion*

As discussed, the acquisition of pre and postoperative motion is not optimal. The Euclidean distance is not the best criterion for range of motion and cannot be used as a validation for the biomechanical model. The coordinates are measured in camera coordinates and are thus not aligned to the subjects head. Coordinates can be aligned in one direction by taking the corners of the subject's eyes. The other directions are more difficult to detect as there is no solid point to calibrate the depth and horizontal turning of the head. Although not completely solid, the marker on the nose could be used to try and determine depth and rotation of the head. Another suggestion is to use a calibration tool mounted to the face of the patient under both pre and postoperative conditions. Alternatively, it could also be a small plate with mounted coordinate axis for the patient to bite on. Another point of discussion was that the movement of the jaw is not recorded. This can be fixed by simply adding a marker on the chin to compensate for jaw movements.

5.6 *Creation of the complete airway structure*

The final aim of virtual surgery is not the prediction of postoperative motion, but the prediction of postoperative functional performance. To predict speech and swallowing outcomes the complete vocal tract have to be modelled. Ongoing research at the University of British Columbia is focused on the modelling the complete upper airways and digestive tract. Eventually, this model will be able to transfer fluid and solid boluses just like a real human. A speech synthesizer will also be built in to simulate speech. A postoperative tongue model could be implemented in the model to explore the effects of the impairment of the tongue on postoperative speech and swallowing function. After the tongue is sufficiently personalised, implementing the tongue in such a model and simulate the effects of surgery or radiation would be the final aim for this project

5.7 *Comparison with expertise of surgeon*

As can be read in Appendix G an additional study was started to gather predictions of functional outcome from surgeons just

before surgery. When the collection is complete, predicted surgical outcome from the virtual surgery could be compared with the prediction of the surgeon. It would be the ultimate validation for the biomechanical model. Only when the biomechanical model is able to predict functional outcome better than a surgeon it would be an addition to clinical practice.

6. REFERENCES

1. Integraal Kankercentrum Nederland. dutch cancer figures. <http://www.cijfersoverkanker.nl/>. Published 2016. Accessed May 11, 2016.
2. Jin Gao Newell W, Johnson, Scott Coman, Alan R. Clough BP. Basic consideration of research strategies for head and neck cancer. *Front Med*. 6(4):339-353. <http://journal.hep.com.cn/fmd>.
3. de Vries N, van de Heyning PH, Leemans CR. *Leerboek Keel-Neus-Oorheelkunde En Hoofd-Halschirurgie*. Bohn Stafleu van Loghum; 2013.
4. Rosebush MS, Rao SK, Samant S, et al. Oral cancer: enduring characteristics and emerging trends. *J Tenn Dent Assoc*. 2011;91(2):24-27; quiz 28-29.
5. Blot WJ, McLaughlin JK, Winn DM, et al. Smoking and Drinking in Relation to Oral and Pharyngeal Cancer. *Cancer Res*. 1988;(48):3282-3287.
6. Neville BWDD, Allen CM, Bouquet JE. *Oral and Maxillofacial Pathology*. St. Louis, MO.; 2009.
7. Appleby P, Beral V, Berrington De González A, et al. Carcinoma of the cervix and tobacco smoking: Collaborative reanalysis of individual data on 13,541 women with carcinoma of the cervix and 23,017 women without carcinoma of the cervix from 23 epidemiological studies. *Int J Cancer*. 2006;118(6):1481-1495. doi:10.1002/ijc.21493.
8. Silva SD Da, Ferlito A, Takes RP, et al. Advances and applications of oral cancer basic research. *Oral Oncol*. 2011;47(9):783-791. doi:10.1016/j.oraloncology.2011.07.004.
9. Matsui Y, Ohno K, Yamashita Y, Takahashi K. Factors influencing postoperative speech function of tongue cancer patients following reconstruction with fasciocutaneous/myocutaneous flaps-a multicenter study. *Int J Oral Maxillofac Surg*. 2007;36(7):601-609. doi:10.1016/j.ijom.2007.01.014.
10. Suarez-Cunqueiro M-M, Schramm A, Schoen R, et al. Speech and swallowing impairment after treatment for oral and oropharyngeal cancer. *Arch Otolaryngol Head Neck Surg*. 2008;134(12):1299-1304. doi:10.1001/archotol.134.12.1299.
11. Borggrevén PA, Aaronson NK, Verdonck-de Leeuw IM, et al. Quality of life after surgical treatment for oral and oropharyngeal cancer: A prospective longitudinal assessment of patients reconstructed by a microvascular flap. *Oral Oncol*. 2007;43(10):1034-1042. doi:10.1016/j.oraloncology.2006.11.017.
12. Lee DY, Ryu YJ, Hah JH, Kwon TK, Sung MW, Kim KH. Long-term subjective tongue function after partial glossectomy. *J Oral Rehabil*. 2014;41(10):754-758. doi:10.1111/joor.12193.
13. Chuanjun C, Zhiyuan Z, Shaopu G, Xinquan J, Zhihong Z. Speech after partial glossectomy: A comparison between reconstruction and nonreconstruction patients. *J Oral Maxillofac Surg*. 2002;60(4):404-407. doi:10.1053/joms.2002.31228.
14. Kreeft a., Tan IB, Van Den Brekel MWM, Hilgers FJ, Balm a. JM. The surgical dilemma of “functional inoperability” in oral and oropharyngeal cancer: Current consensus on operability with regard to functional results. *Clin Otolaryngol*. 2009;34(2):140-146. doi:10.1111/j.1749-4486.2009.01884.x.
15. van Dijk S, van Alphen MJA, Jacobi I, Smeele LE, van der Heijden F, Balm AJM. A New Accurate 3D Measurement Tool to Assess the Range of Motion of the Tongue in Oral Cancer Patients: A Standardized Model. *Dysphagia*. 2016;31(1):97-103. doi:10.1007/s00455-015-9665-7.
16. Kiritani S, Miyawaki K, Fujimura O, Miller JE. Computational model of the tongue. In: New Jersey, Hongo Tokyo; 1975.
17. Gerard J-M, Wilhelms-Tricarico R, Perrier P, Payan Y. A 3D dynamical biomechanical tongue model to study speech motor control. 2003:1-18. <http://arxiv.org/abs/physics/0606148>.
18. Gérard J-M, Perrier P, Payan Y. 3D biomechanical tongue modeling to study speech production. *Speech Prod Model Phonetic Process Tech*. 2006:85-102. <http://hal.archives-ouvertes.fr/hal-00108521/>.
19. Van Alphen MJA, Kreeft AM, Van Der Heijden F, Smeele LE, Balm AJM. Towards virtual surgery in oral cancer to predict postoperative oral functions preoperatively. *Br J Oral Maxillofac Surg*. 2013;51(8):747-751. doi:10.1016/j.bjoms.2013.06.012.
20. Vogt F, Lloyd J, Buchaillard S, et al. Efficient 3d finite element modeling of a muscle-activated tongue. *Lect notes Comput Sci*. 2006;(4072):19-28.
21. Fujita S, Dang J, Suzuki N, Honda K. A Computational Tongue Model and its Clinical Application. *Oral Sci Int*. 2007;4(2):97-109. doi:10.1016/S1348-8643(07)80004-8.
22. Buchaillard S, Brix M, Perrier P, Payan Y. Simulations of the consequences of tongue surgery on tongue mobility: Implications for speech production in post-surgery conditions. *Int J Med Robot + Comput Assist Surg*. 2007;(3):252-261. doi:10.1002/rcs.142.
23. Buchaillard S, Perrier P, Payan Y. A biomechanical model of cardinal vowel production: muscle activations and the impact of gravity on tongue positioning. *J Acoust Soc Am*. 2009;126(4):2033-2051. doi:10.1121/1.3204306.
24. van Dijk S, van Alphen MJ., Smeele LE, van der Heijden F, Balm AJM. Tongue mobility assessment in oral cancer patients using a new 3D measurement tool: Towards a predictive model. In: *AHNS 10th International Conference on Head and Neck Cancer*. ; 2016.
25. Stavness I, Lloyd JE, Fels S. Automatic prediction of tongue muscle activations using a finite element model. *J Biomech*. 2012;45(16):2841-2848. doi:10.1016/j.jbiomech.2012.08.031.
26. Lloyd JE, Stavness I, Fels S. ArtiSynth: A Fast Interactive Biomechanical Modeling Toolkit Combining Multibody and Finite Element Simulation. *Soft Tissue Biomech Model Comput Assist Surg*. 2012:355-394. doi:10.1007/8415_2012_126.
27. MeshLab - Visual Computing Lab - ISTI - CNR. <http://meshlab.sourceforge.net/>.
28. Wilhelms-Tricarico R. Development of a tongue and mouth floor model for normalization and biomechanical modelling,” in Proceedings of the Fifth Speech Production Seminar and CREST Workshop on Models of Speech Production. In: Kloster Seoon, Bavaria; 2000.

29. Slaughter K, Li H, Sokoloff AJ. Neuromuscular Organization of the Superior Longitudinalis Muscle in the Human Tongue. *Cells Tissues Organs*. 2005;181(1):51-64. doi:DOI/10.1159/000089968.
30. Stavness I, Lloyd JE, Payan Y, Fels S. Coupled hard-soft tissue simulation with contact and constraints applied to jaw-tongue-hyoid dynamics. *Int j numer method biomed eng*. 2011;27(3):367-390. doi:10.1002/cnm.1423.
31. Boy S, Guennebaud G, Schlick C, et al. Least Squares Subdivision Surfaces. *Comput Graph Forum (Proceedings Pacific Graph 2010)*, Wiley-Blackwell. 2010.
32. Fung YC. *Biomechanics: Mechanical Properties of Living Tissue*. Springer-Verlag; 1993.
33. Gerard JM, Ohayon J, Luboz V, Perrier P, Payan Y. Non-linear elastic properties of the lingual and facial tissues assessed by indentation technique: Application to the biomechanics of speech production. *Med Eng Phys*. 2005;27(10):884-892. doi:10.1016/j.medengphy.2005.08.001.
34. Duck FA. *Physical Properties of Tissues: A Comprehensive Reference Book*. London; 1990.
35. Blemker SS, Pinsky PM, Delp SL. A 3D model of muscle reveals the causes of nonuniform strains in the biceps brachii. *J Biomech*. 2005;38(4):657-665. doi:10.1016/j.jbiomech.2004.04.009.
36. C. Criscione J, S. Douglas A, C. Hunter W. Physically based strain invariant set for materials exhibiting transversely isotropic behavior. *J Mech Phys Solids*. 2001;49(July):871-897. doi:10.1016/S0022-5096(00)00047-8.
37. Stavness IK. *Byte Your Tongue: A Computational Model of Human Mandibular-Lingual Biomechanics for Biomedical Applications*. 2010.
38. Bushell DGT and MC. The spatial mapping of translational diffusion coefficients by the NMR imaging technique. *Phys Med Biol*. 1985;30(4):345.
39. Gilbert RJ, Wedeen VJ, Magnusson LH, et al. Three-dimensional myoarchitecture of the bovine tongue demonstrated by diffusion spectrum magnetic resonance imaging with tractography. *Anat Rec - Part A Discov Mol Cell Evol Biol*. 2006;288(11):1173-1182. doi:10.1002/ar.a.20387.
40. Gaije TA, Benner T, Wang R, Wedeen VJ, Gilbert RJ. Three dimensional myoarchitecture of the human tongue determined in vivo by diffusion tensor imaging with tractography. *J Magn Reson Imaging*. 2007;26(3):654-661. doi:10.1002/jmri.21022.
41. Rohan P-Y, Lobos C, Nazari M a., Perrier P, Payan Y. Finite element models of the human tongue: a mixed-element mesh approach. *Comput Methods Biomech Biomed Eng Imaging Vis*. 2016;00(March):1-11. doi:10.1080/21681163.2015.1105760.
42. Agur A, Dalley A. *Grant's Atlas of Anatomy*. 11th ed. Wolters Kluwer, Lippincott Williams & Wilkins; 2005.
43. Takemoto H. Morphological Analyses of the Human Tongue Musculature for Three-Dimensional Modeling. *J Speech, Lang Hear Res*. 2001;44(1):95-107. [http://dx.doi.org/10.1044/1092-4388\(2001/009\)](http://dx.doi.org/10.1044/1092-4388(2001/009)).
44. teachmeanatomy.org.
45. <https://classconnection.s3.amazonaws.com/844/flashcards/2475844/png/verticalmuscle1355942078479.png>.
46. Khennane A. *Introduction to Finite Element Analysis Using MATLAB and Abaqus*. Taylor & Francis Group, LLC; 2013. doi:10.1201/b15042.
47. Nikishkov G. *Programming Finite Elements in Java*. Vol 1. Aizu-Wakamatsu, Japan: Springer; 2010. doi:10.1017/CBO9781107415324.004.
48. Si H. TetGen, a Quality Tetrahedral Mesh Generator. *AMC Trans Math Softw*. 2015;41(2):11. doi:10.1007/3-540-29090-7_9.
49. Schonning A, Oommen B, Ionescu I, Conway T. Hexahedral mesh development of free-formed geometry: The human femur exemplified. *CAD Comput Aided Des*. 2009;41(8):566-572. doi:10.1016/j.cad.2007.10.007.
50. Huang Y, White DP, Malhotra A. Use of Computational Modeling to Predict Responses to Upper Airway Surgery in Obstructive Sleep Apnea. *Laryngoscope*. 2007;117(4):648-653. doi:10.1097/MLG.0b013e318030ca55.
51. Lloyd JE. *ArtiSynth Reference Manual*. July 8. [http://artisyntn.magic.ubc.ca/pmwiki.php?n=Documentation.Artisyntn thRefManual](http://artisyntn.magic.ubc.ca/pmwiki.php?n=Documentation.Artisyntn%20thRefManual). Published 2014. Accessed August 5, 2016.
52. Rinkel R, Leeuw I, Reij E van. Speech handicap index in patients with oral and pharyngeal cancer: better understanding of patients' complaints. *Head* 2008;(July):868-874. doi:10.1002/hed.
53. List MA, Ritter-Sterr C LS. A Performance Status Scale for Head and Neck Cancer Patients. *Cancer*. 1990;(66):564-569.
54. Ackerstaff A, Tan I. Quality-of-life assessment after supradose selective intra-arterial cisplatin and concomitant radiation (RADPLAT) for inoperable stage IV head and neck. *Arch Otolaryngol Head Neck Surg*. 2002;128(10):1185-1190. doi:10.1001/archotol.128.10.1185.
55. van der Molen L, van Rossum MA, Jacobi I, et al. Pre- and posttreatment voice and speech outcomes in patients with advanced head and neck cancer treated with chemoradiotherapy: expert listeners' and patient's perception. *J Voice*. 2012;26(5):664.e25-e33. doi:10.1016/j.jvoice.2011.08.016.
56. Chen A. The development and validation of a dysphagia-specific quality-of-life questionnaire for patients with head and neck cancer: the MD Anderson dysphagia inventory. *Arch Otolaryngol Head Neck Surg*. 2001;(July 2001):870-876. doi:10-1001.

Appendix A. ANATOMY OF THE TONGUE

The tongue is a complex structure, solely made of muscles. The muscles can be divided into two groups. Extrinsic muscles originate from a ridged structure and are named after a ridged structure or the location of the muscle. Intrinsic muscles only have muscle-muscle contact and are named after the way they course. Table 8 shows a summary of the muscles.

Table 8: Table of Extrinsic and intrinsic muscles of the tongue.

Extrinsic muscles	Intrinsic muscles
Genioglossus (GG)	Superior longitudinal muscle (SL)
Hyoglossus (HG)	Inferior longitudinal muscle (IL)
Styloglossus (STY)	Transverse muscle (TRANS)
Palatoglossus*	Vertical muscle (VERT)
Geniohyoidus (GH)**	
Mylohyoid Muscle (MH)**	

*The palatoglossus is not simulated in the biomechanical model
 ** these are muscles from the floor of mouth, but are also embedded in the biomechanical models

Extrinsic muscles

The main action of the **M. Genioglossus (GG)** is to depress the tongue. Its posterior part pulls the tongue towards anterior for protrusion. The GG originates anteriorly from the mental spines on the inner surface of the mandibula. As can be seen in figure 1, the GG fans out over a great part of the tongue and intersects with the **Superior longitudinal muscle (SL)**. A smaller part is also connected to the hyoid bone. Caudal from the GG is the longitudinal **M. Geniohyoidus (GH)** which is connected to both the mental spines and the hyoid bone. This muscle brings the hyoid bone forward and upwards causing dilatation of the upper airway, used during respiration. The **M. Styloglossus (SG)** is originated from the distal part of the styloid process. Its function is to retract and draw up the tongue to create a passageway for swallowing. The **M. Hyoglossus (HG)** originates from the hyoid bone and contracts or depresses the tongue. Innervation of the most extrinsic muscles is controlled by branches of the hypoglossal nerve (XII). An exception is the **Palatoglossus (PG)**, which is innervated by the vagus nerve. The PG elevates the posterior part of the tongue and is not necessary needed for swallowing^{42,43}. The **mylohyoid muscle (MH)** is not a part of the tongue but forms the floor of mouth. The muscle has its origin at the medial side of the mandible and its insertions at the hyoid bone and the mandibular symphysis. The MH can elevate the tongue and is an important muscle during swallowing and speech. Innervation is performed by the Mandibular branch of trigeminal nerve (V)^{42,43}

Intrinsic Muscles

The **superior longitudinal muscle** is located inferior to the lamina propria in the tongue dorsum and curls the tip and sides of the tongue when innervated. It also shortens the tongue. The **Inferior longitudinal muscle (IL)** is located lateral from the GG. It also serves to curl the tongue but from a deeper muscle layer. Both the **transversers and the vertical muscles** are located caudal from the SL and proximal from the IL. The fibres from the transverse muscle travel from the medial septum to the lateral border of the tongue. The fibres from the vertical muscle travel from the ventrolateral submucosa to the dorsum of the tongue. All intrinsic muscles are innervated by the hypoglossal nerve.^{42,43}

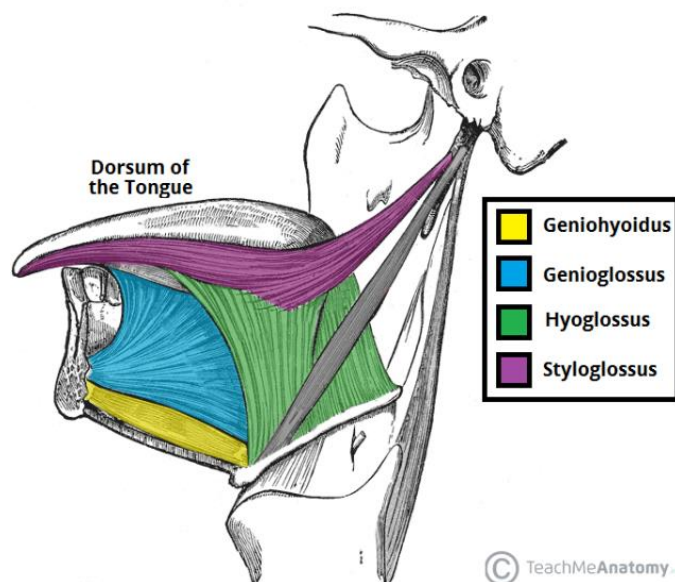


Figure 23: Sagittal anatomical illustration of tongue muscles⁴⁴.

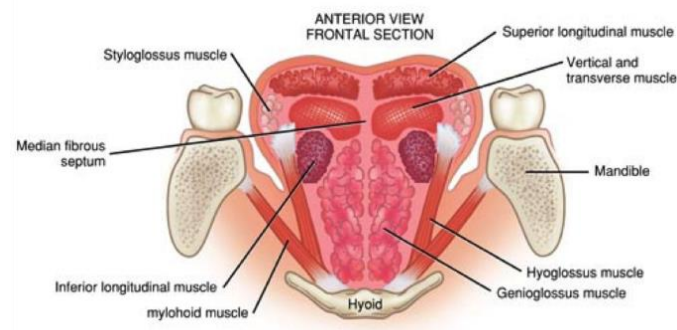


Figure 24: coronal illustration of tongue muscles⁴⁵.

Appendix B. THE VIRTUAL THERAPY PROJECT

The goal of Virtual Therapy is to find balance between cure and quality of life in patients suffering from head and neck cancer. Right now this is difficult because postoperative functional outcomes such as swallowing, mastication and speech are hard to predict accurately. The choice for treatment is therefore based on a hard threshold in a grey area.

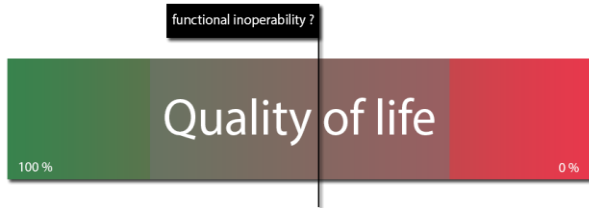


Figure 25: illustration that points out that functional inoperability is a hard threshold in a large grey and unknown area which is quality of life.

The Virtual Therapy Project is aimed at clearing up this grey area and to provide tools to both the physician and patient to make decisions based on accurate predictions of function outcome. The most promising tool will be a biomechanical model that is able to simulate the patients individual aero digestive tract pre and postoperative. The tool will be focused on the main functionalities of this tract:

- Swallowing
- Mastication
- Speech

The project is aimed at the construction of a personal biomechanical model of the patients aero digestive tract after the first consultation. The surgeon or clinical technician will then simulate different kinds / combinations of treatments which can be evaluated at the multidisciplinary board meeting. The patient will be confronted with a model that shows its own postoperative functional impairment (Figure 26). The patient will also be able to hear the predicted changes in voice. This can make the patient better informed to make its own decision and to choose for the other treatment option if available. Creating this biomechanical model is a long term goal, as many steps towards this goal are not straight forward or easy.

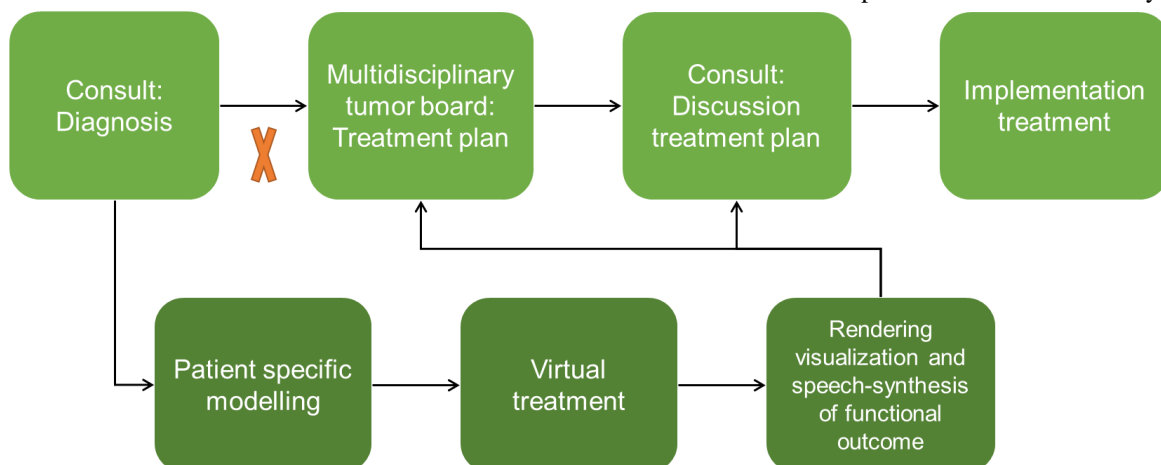


Figure 26: An illustration showing the proposed clinical work-up.

Requirements

Important anatomical structures that are involved in these functionalities and thus need to be simulated are:

- Lips / muscles of the face
- Oral cavity: lips / Tongue / floor of mouth
- Oropharynx: palate and soft palate
- Larynx and hypopharynx: Vocal cords / epiglottis

Each anatomical structure has its own contribution to these functionalities. Only when the contributions of all individual structures are known, a complete functionality model can be made. In addition, anatomical changes and compensatory movements after an intervention have to be taken into account.

pre intervention: Initial state of the model

In order to simulate effects of an intervention, the initial model needs to resemble the patient as close as possible. Methods need to be developed to personalise the anatomical shapes of the structures, but also there preoperative functionality. Muscle force, the direction of muscle fibres and tissue properties are all needed to get a good representation of the functionalities of structures. Techniques used in this part of the developed are segmentation and 3D morphing of medical imaging, functional EMG to measure muscle contribution, Dynamic Tensor Imaging (DTI) and video tracking tools.

During intervention: State change

The most important question during the intervention is: what is changing and how is it changing? Tools need to be developed to change the preoperative model in such a way that it resembles interventions such as surgery, radiation and photodynamic therapy. Therefore the effects of different interventions on different structures need to be clear and implemented. This includes the effect of retraction after suturing the resection, but also the generation of fibrous tissue after surgery and/or radiotherapy. When an intervention is sufficiently imitated the outcome is also highly dependent on how advance the personalisation of the initial state was. Another important part of this phase is the interaction with the physician. The tool must be able to alter the state of the initial model in the way the physician wants it to be. This means that a large amount of work also includes the development of interfaces and ways to interact

with the model. All these aspects should not be too time consuming to allow a timely construction of a virtual surgery tool. Techniques such as video / Electromagnetic motion tracking and fluoroscopy could help us understand more of the processes involved.

After intervention: The functional outcome

After the invention the personalised model of the patient is changed. For the functional outcome, methods need to be developed to use the altered model to demonstrate the functional differences after surgery. Therefore methods are needed that can simulate air and fluid flow in the supralaryngeal digestive tract, but also transport of more solid structures. Postoperative shapes of the lips and tongue need to be connected to speech production and mastication to generate an objective measure for quality of life. All simulated functions should be fully comprehensible for the individual patient.

Appendix C. THE FINITE ELEMENT METHOD

one-dimensional finite element approximation

FEM is a method used to make highly complex mechanical problems, solvable by dividing a structure into several smaller structures. It is a method often used in mechanical engineering to solve thermal problems, fluid problems and mechanical problems. A continuous physical problem is transformed into a discretised finite element problem. An element is a 1D, 2D or 3D interpolated line/area/volume bound by nodes. These nodes are divided as discrete positions and “carry” the mechanical fields. Values within finite elements can be recovered by interpolating nodal values. For a linear problem a system of linear algebraic equations (contained within nodes) should be assembled and solved.

The main steps of the finite element solution procedure are:

1. Discretize the domain: divide a domain (the object) into finite elements and nodes.
2. Determine interpolation functions: Polynomials are selected as interpolation function. The degree of these functions depends on the number of nodes per element. This function is also called the shape function as it usually determines the shape of the element. Examples are Tetrahedral, Hexahedral elements.
3. Compute element matrix and vectors: The matrix equation that relates the nodal values of the unknown function to the known parameters is created.
4. Assembling of element equations: Local element equations need to be combined properly to find a global equation system. Elements connectivity's are used in this process and also boundary conditions should be imposed.
5. Solve the global equation system: Direct and Iterative methods can be used the find nodal values.

To understand the principle of Finite Element its best to just start with simple examples. In the next section there will be three examples, each example a bit more advanced.

The simplest way to explain the finite element method is by analysing a 1D example⁴⁶.

Figure 27 shows an elastic rod with ends 1 and 2. These are the nodes. When a force N_1 is applied to node 1 in the direction of 2 while node 1 is fixed the equation is as follows:

$$N_1 = \frac{AE}{L} u_1 \quad (11)$$

With L the length of the rod, A the cross section, E the Young's modulus and u_1 the amount of shortening.

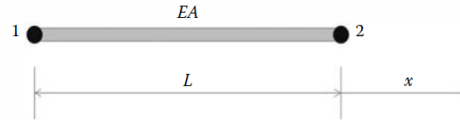


Figure 27: Example of a rod, with nodes 1 and 2, length L and cross sectional area EA⁴⁶.

According to Newton's 3th law there must be a reaction force R_2 at node 2 N_2 That is the opposite of N_1 .

If we add a force N_2 at node 2 pointing away from node 1 the rod lengthens by an amount u_2 . The reaction force R_1 will be the opposite of R_2 .

When the rod is subjected to both forces N_1 and N_2 the total forces F_1 will be:

$$F_1 = N_1 - R_1 = \frac{AE}{L} u_1 - \frac{AE}{L} u_2 \quad (12)$$

$$F_2 = N_2 - R_2 = -\frac{AE}{L} u_1 + \frac{AE}{L} u_2 \quad (13)$$

And in vector from:

$$\begin{bmatrix} \frac{AE}{L} & -\frac{AE}{L} \\ \frac{AE}{L} & \frac{AE}{L} \end{bmatrix} \begin{Bmatrix} u_1 \\ u_2 \end{Bmatrix} = \begin{Bmatrix} F_1 \\ F_2 \end{Bmatrix} \quad (14)$$

Or as a simpler equation:

$$[K_e] \{u_e\} = \{F_e\} \quad (15)$$

With $\{u_e\}$ the nodal displacements and $\{F_e\}$ the nodal forces.

$[K_e]$ is called the stiffness matrix.

As can be seen in the picture; without constraints there will be no single solution to this system. This makes sense as one can imagine the rod will move in space when the 2 unknown forces F_1 and F_2 are applied. Now in the same way a more complex structure will be discussed:

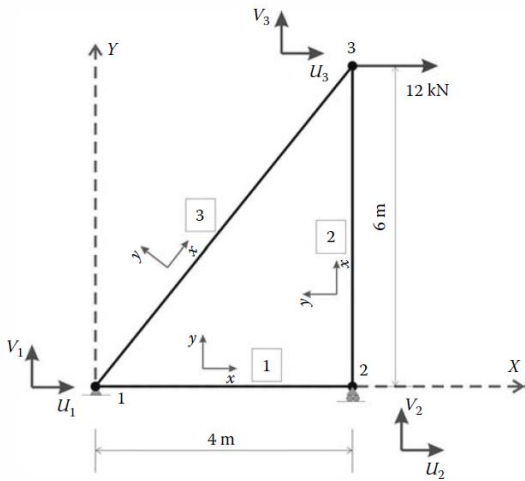


Figure 28: Example of a structure consisting of 3 nodes and 3 elements. Also boundary conditions are applied⁴⁶.

This is a simple structure consisting of three nodes and three elements. Only axial movement is possible, so each node has 2 degrees of freedom. The total system thus has 6 degrees of freedom. As boundary conditions we say that 1 is fixed, 2 is a rolling element on the X-axis and 3 is free. An element consist of 2 nodes and thus 4 degrees of freedom:

$$\{d_e\} = \{u_1, v_1, u_2, v_2\}^T \quad (16)$$

The stiffness matrix for that element is of the form:

$$[K_e] = \begin{bmatrix} \frac{AE}{L} & 0 & -\frac{AE}{L} & 0 \\ 0 & 0 & 0 & 0 \\ -\frac{AE}{L} & 0 & \frac{AE}{L} & 0 \\ 0 & 0 & 0 & 0 \end{bmatrix} \quad (17)$$

The elements only have axial deformation so the second and fourth column, representing transversal deformation, are zero. To make the next section clear, it is easier to use actual numbers for the calculation. Let's assume that these elements are made of platinum, with a Young's modulus of Platinum (21300MPa) a fictional cross-sectional area of 2000 mm² (A.) With this we can calculate for example the stiffness matrix of element 2:

$$[K_2] = \begin{bmatrix} 7100 & 0 & 7100 & 0 \\ 0 & 0 & 0 & 0 \\ 7100 & 0 & 7100 & 0 \\ 0 & 0 & 0 & 0 \end{bmatrix} \quad (18)$$

Element 1 and 3 are calculated in the same way.

Global stiffness matrix

Now that we have the stiffness matrix of the three elements, they need to be assembled to a global stiffness matrix. As can be seen in figure x, the local coordinate system of element 1 is the same as that of the global system. $U_1 = X$ and $V_1 = Y$. Element 2 has an angle of 90° with the global coordinate system. The stiffness matrix of element 2 in global coordinates

can be calculated using a transformation matrix $[C]$ and the following formula:

$$[\overline{K}_e] = [C][K_e][C]^T \quad (19)$$

$[\overline{K}_e]$ is the stiffness matrix of the global coordinate system. The transformation matrix is:

$$[C] = \begin{bmatrix} \cos 90 & -\sin 90 & 0 & 0 \\ \sin 90 & \cos 90 & 0 & 0 \\ 0 & 0 & \cos 90 & -\sin 90 \\ 0 & 0 & \sin 90 & \cos 90 \end{bmatrix} = \begin{bmatrix} 0 & -1 & 0 & 0 \\ 1 & 0 & 0 & 0 \\ 0 & 0 & 0 & -1 \\ 0 & 0 & 1 & 0 \end{bmatrix} \quad (20)$$

So $[\overline{K}_2]$ is:

$$[\overline{K}_2] = \begin{bmatrix} 0 & 0 & 0 & 0 \\ 7100 & 0 & 7100 & 0 \\ 0 & 0 & 0 & 0 \\ -7100 & 0 & 7100 & 0 \end{bmatrix} \quad (21)$$

This is also done with element 3 resulting in:

$$[\overline{K}_3] = \begin{bmatrix} 1818 & 2727 & -1818 & -2727 \\ 2727 & 4090 & -2727 & -4090 \\ -1818 & -2727 & 1818 & 2727 \\ -2727 & -4090 & 2727 & 4090 \end{bmatrix} \quad (22)$$

Combining $[\overline{K}_1]$, $[\overline{K}_2]$ and $[\overline{K}_3]$ into one global stiffness matrix gives:

$$[K] = \begin{bmatrix} 12468 & 2726 & -10650 & 0 & -1818 & -2727 \\ 2727 & 4090 & 0 & 0 & -2727 & -4090 \\ -10650 & 0 & 10650 & 0 & 0 & 0 \\ 0 & 0 & 0 & 7100 & 0 & 7100 \\ -1818 & -2727 & 0 & 0 & 1818 & 2727 \\ -2727 & -4090 & 0 & -7100 & 2727 & 11190 \end{bmatrix} \quad (23)$$

Boundary conditions:

To get a unique solution for the question. boundary conditions are needed. Because in this case Node 1 is completely fixed and node 2 partially (roller) it is possible to calculate an unique solution for this case. This solution is completely explained in: "Introduction to Finite Element Analysis Using MATLAB and Abaqus" of A Khennane⁴⁶. In this simple example we discussed the principles of working towards an solution of a finite element problem. It is now clear how to how to give physical properties to nodes and how to assemble the global stiffness matrix. Also without boundary conditions, there will be no unique solution. The next example will be more comparable to the Finite Element used in the tongue model:

FEM of a solid structure.

This example shows an 3D elastic body structure that is subjected to body forces p^x , body forces p^y , A temperature field T and displacement u^s . This example is based on "Programming Finite Elements in Java" from G. Nikishkov⁴⁷.

$$\{\varepsilon\} = \{\varepsilon_x \varepsilon_y \varepsilon_z \varepsilon_{xy} \varepsilon_{xz} \varepsilon_{zx}\} \quad (30)$$

The relationship between strains and displacement is:

$$\{\varepsilon\} = [B]\{q\} \quad (31)$$

With B the displacement differentiation matrix which is defined as:

$$[B] = [D][N] \quad (32)$$

With D the matrix differentiation operator:

$$[D] = \begin{bmatrix} \frac{\partial}{\partial x} & 0 & 0 \\ 0 & \frac{\partial}{\partial y} & 0 \\ 0 & 0 & \frac{\partial}{\partial z} \\ \frac{\partial}{\partial y} & \frac{\partial}{\partial x} & 0 \\ 0 & \frac{\partial}{\partial z} & \frac{\partial}{\partial y} \\ \frac{\partial}{\partial z} & 0 & \frac{\partial}{\partial x} \end{bmatrix} \quad (33)$$

Using the shape function and matrix differentiation operator the displacement differentiation matrix can be made:

$$[B_i] = \begin{bmatrix} \frac{\partial N_i}{\partial x} & 0 & 0 \\ 0 & \frac{\partial N_i}{\partial y} & 0 \\ 0 & 0 & \frac{\partial N_i}{\partial z} \\ \frac{\partial N_i}{\partial y} & \frac{\partial N_i}{\partial x} & 0 \\ 0 & \frac{\partial N_i}{\partial z} & \frac{\partial N_i}{\partial y} \\ \frac{\partial N_i}{\partial z} & 0 & \frac{\partial N_i}{\partial x} \end{bmatrix} \quad (34)$$

Stresses (stress vector $\{\sigma\}$) are related to strains in elastic body by Hooke's Law:

$$\{\sigma\} = [E]\{\varepsilon^e\} = [E](\{\varepsilon\} - \{\varepsilon^t\}), \quad (35)$$

$$\{\varepsilon^t\} = \{\alpha T \ \alpha T \ \alpha T \ 0 \ 0 \ 0\} \quad (36)$$

E is the elasticity matrix which depends on elastic material properties. $\{\varepsilon\}$ is the elastic part of strains and $\{\varepsilon^t\}$ the thermal part. $[E]$ is the elasticity matrix which depends on the elastic

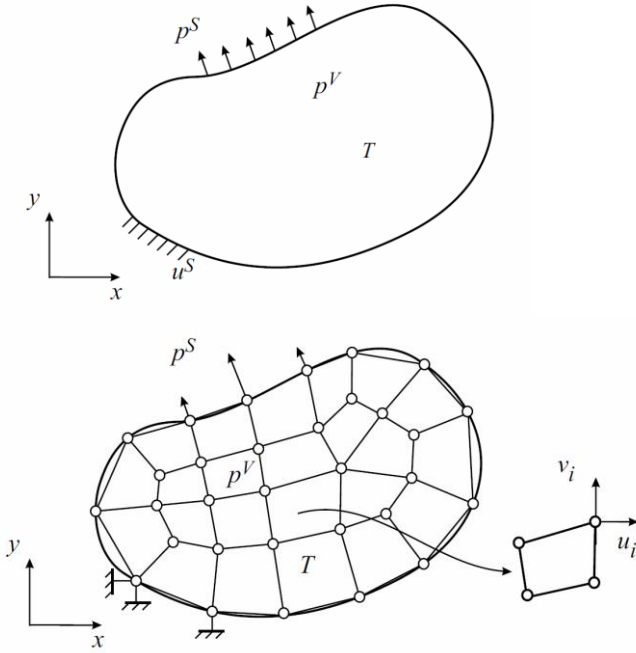


Figure 29: discretised domain of an elastic body structure⁴⁷.

The first step is to discretise the domain (Figure 29). So using nodes, quadrilateral elements will be created that resemble the shape of the original model as much as possible. Constraints are being coupled to the nodes in the lower left corner. Three of the upper nodes will have forces that point in a certain direction. All properties of this object are now related to the nodal points. First the element equation needs to be found:

The nodal displacement along x,y,z is be formulated as:

$$\{q\} = \{u_1 \ v_1 \ w_1 \ u_2 \ v_2 \ w_2 \ \dots\} \quad (24)$$

Displacement $\{u\}$ at some point in the finite element can be found using $\{q\}$ and the shape function N_i :

$$u = \sum N_i u_i \quad (25)$$

$$v = \sum N_i v_i \quad (26)$$

$$w = \sum N_i w_i \quad (27)$$

This can be rewritten in matrix form:

$$\{u\} = [N]\{q\} \quad (28)$$

With N, the shape function:

$$[N] = \begin{bmatrix} N_1 & 0 & 0 & N_2 & \dots \\ 0 & N_1 & 0 & 0 & \dots \\ 0 & 0 & 0 & N_1 & \dots \end{bmatrix} \quad (29)$$

Strains can be determined through displacements at nodal points. The strain vector consist of 6 strain components:

properties of the material. α is the thermal expansion coefficient and T the temperature.

The goal of the finite element solution of an elastic problem is to find a displacement field in the potential energy Π in the system is minimal:

$$\Pi = \int_V \frac{1}{2} \{\varepsilon^e\}^T \{\sigma\} dV - \int_V \{u\}^T \{P^V\} dV - \int_S \{u\}^T \{P^S\} dS \quad (37)$$

$\{P^V\}$ is the body force vector and $\{P^S\}$ the surface forces. Using the stress and strain relations the total potential energy through nodal displacements can be expressed as:

$$\Pi = \int_V \frac{1}{2} ([B]\{q\} - \{\varepsilon^t\})^T [E] ([B]\{q\} - \{\varepsilon^t\}) dV - \int_V [N]\{q\}^T \{P^V\} dV - \int_S [N]\{q\}^T \{P^S\} dS \quad (38)$$

The nodal displacements $\{q\}$ correspond to the minimum of the functional Π are determined by the condition:

$$\left\{ \frac{\partial \Pi}{\partial q} \right\} = 0. \quad (39)$$

After differentiation from Π with respect to $\{q\}$ it gives the following equilibrium equation for a finite element:

$$\int_V [B]^T [E] [B] dV - \int_V [B]^T [E] \{\varepsilon^t\} dV - \int_V [N]^T \{P^V\} dV - \int_S [N]^T \{P^S\} dS = 0 \quad (40)$$

Which can be expressed in the same way as equation 15:

$$[k]\{q\} = \{f\} \quad (41)$$

With

$$\{f\} = \{p\} + \{h\}$$

the load vector (force),

$$[k] = \int_V [B]^T [E] [B] dV$$

the Element stiffness matrix,

$$\{p\} = \int_V [N]^T \{P^V\} dV - \int_S [N]^T \{P^S\} dS$$

the vector of the actual forces and

$$\{h\} = \int_V [B]^T [E] \{\varepsilon^t\} dV$$

the thermal vector (represents frictions forces).

We now have the same expression as in example 1 but for an elastic 3D body. The next step is the assembly of the global equation system and finding a solution for the complete system. For previous example this is explained in “Programming finite elements in java” from G. Nikishkov⁴⁷

In these examples we have discussed all steps of the finite element analysis in a non-structured way. We did not solve any of the examples because this is usually a substantial effort by hand. For this purpose a lot of software solutions such as ANSYS, Abaqus and ArtiSynth are available. In programming different solvers can be used to solve these differential equations for large systems. More about these integrators can be read in Appendix E.

Appendix D. FINITE ELEMENT MESHING TECHNIQUES

As mentioned multiply times the initial tongue model in Artisynt based on Buchaillard et al. (2009)²³ is completely handmade. Implementing the surgery tool required editing of the model. Before S. Fels (UBC) came up with the idea to split the surface mesh and the FEM model, other methods were explored:

Removing Elements from the original model

The simplest way to perform surgery on the original model was to remove elements using the standard editing tool in ArtiSynth. Visual inspection of the model (Figure 30) shows that removing these structures hardly resembles a real resection because of the sharp edges and flat bottom. Because of the large elements, it is not possible to create complex resection shapes. Closing this hole using the same suturing technique as in this thesis would lead to an unstable model and is therefore not possible. The advantage of this method, however, was that the original fibre muscles could be used. Also, the rest of the original model would stay unchanged and therefore no validation of the new model was needed. Surgery on this model using free-flap reconstruction was already performed in Buchaillard(2007)²²

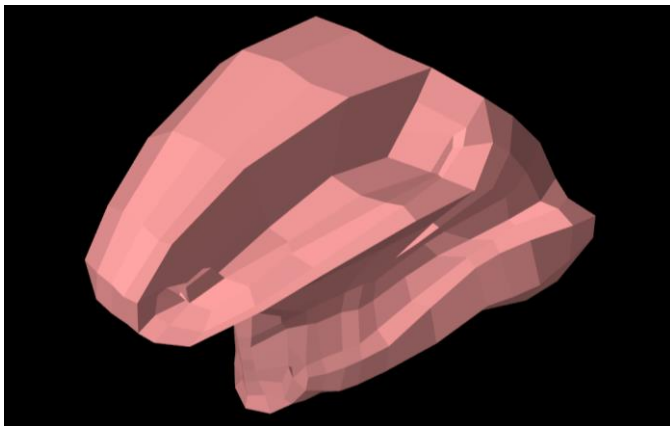


Figure 30: Postoperative model after deleting elements from the initial model.

Changing the FEM shape

In order to get a realistic resection area the FEM mesh needed to change. Nodes always need to connect with a node from another Element. Its therefore not possible to cut elements in half or in other shapes. For this reason there is no good technique today that can automatically generate a hexahedral FEM mesh. However there are techniques to automatically generate tetrahedral meshes. Built-in in Artisynt is the automatic FEM generator TetGen⁴⁸. This software generates a tetrahedral FEM mesh from the original surface mesh. The vertices on the surface will be changes to nodes and the whole structure will be filled with more elements and nodes. The initial model was made in hexahedral elements, so it is effortless to just convert the initial surface mesh to a tetrahedral surface mesh. Using the same techniques used in the method

section a resection volume was created in this model and the wound was closed with virtual sutures.

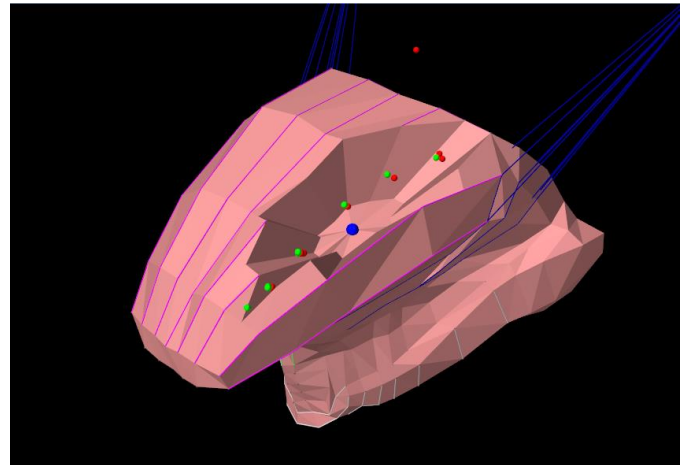


Figure 31: Postoperative model using the TetGen method.

Editing this model was easy, as area's could be generated automatically over and over again. But tetrahedral meshes have some significant disadvantages over hexahedral elements. A reduced convergence of strains and stresses, pressure checkerboard instabilities and mainly: Shear and volumetric locking. This is an artificial stiffening that appears in (almost) compressible materials. As a result of the incompressibility of the material, kinematic constrains force finite elements to deform with a constant volume. This results in a Finite Element model that with degrees of freedom that are not independent anymore.

Ultimately an approach was used in which the surface mesh and FEM model are separate. This is however still an intermediate step. As could be seen in the results, movements are not the same as the initial model and the volume is way larger than the surface mesh. A few recent developments with advanced meshing techniques show promising results.

Advanced meshing techniques

Tetrahedral elements are prone to shear and volumetric locking and are therefore by definition not suitable for hyperelastic materials. Because hexahedral elements are considered the best element shape for hyperelastic materials, hexahedral mesh generation is a popular topic of research. To the present day, this is still a considerable challenge. One of the more recent attempts to create an automated hexahedral mesh is from Schooning et al.⁴⁹ In this paper they tried to create a Femur from only hexahedral elements. Although the creation of this femur succeeded, the writers noted that an extensive amount of human interaction was needed to get the FEM mesh right.

A more promising approach is the mixed-element meshing technique developed by lobos et al (2016)⁴¹. This meshing technique is somewhat similar to what is used in this thesis. The first step is the automated creation of cubic elements according to the shape of a surface mesh. The second step is to fill up the transitions between cubic structures with other elements like tetrahedral element. The result is a FEM model that mainly consist of hexahedral elements, but for a small part of other

elements. In this way the shape of the finite element mesh is matched in the right, way while maintaining the effects of volumetric locking of the tetrahedral elements to a minimum.

These techniques can be used in the future to improve the performance of the FEM mesh that is used during virtual surgery. A mixed mesh approach could be used to create a FEM model that is closer to the shape and volume of the surface mesh than the current one.

Appendix E. INTRODUCTION TO ARTISYNTH

ArtiSynth has been developed at the University of British Columbia for the past several years with speech synthesis in mind. ArtiSynth evolved in a general simulation environment for modelling complex anatomical systems composed of rigid and deformable structures, but many applications are still focused on pathologies of the oral cavity and the upper airway. Sleep apnoea⁵⁰ swallowing disorders, speech pathologies and surgical interventions are all simulated within this environment. ArtiSynth is open source and unlike most of the commercial software available (ANSYS, SIMULA, SolidWorks and ADAMS) ArtiSynth has the ability to create hybrid models (FEM and rigid structures) in an easy way. ArtiSynth consist of an Application Programming Interface (API) for the creation of rigid bodies, joints, FEM, point to point muscles, particles and more. Physics simulations can handle bilateral and unilateral constraints, contact ,friction and inverse simulations. ArtiSynth is built in Java (oracle) and its therefore easy to alter or to extent simulation behaviour. Because Matlab is also working in a java environment, ArtiSynth can be executed by Matlab as well. Matlab is perfectly useful for generating input for biomechanical models, but also for the analysis of these models.

ArtiSynth system design basics

Integration from ArtiSynth with the user is done via a Graphical user interface (GUI) (See Figure 33). This interface consist of play controls, an OpenGL-based viewer, property panels and a timeline. The viewer host the visual representation of the model and tools to edit camera position or other visual properties. Properties of the model that do not change over time can be set in the properties panel. The type of properties that can be set depend on the model that is loaded. Properties are for example: Muscle material, mass, density, damping. For properties that needs to be changed over time, there is the timeline. Let's assume there is a model with certain muscles that can alter the shape of this muscle. To change shape, the muscles need an input signal (excitation signal). The timeline contains those signals visualised as excitation at a certain time. In this example, output can be the location of a certain spot on the model over time. This output is saved to the timeline. The timeline can manage a great amount of in and output signals for each property of the model. Input and output signals are called probes. To advance the model in time a scheduler is used. The scheduler is responsible for the tasks that need to be fulfilled at each time step. The most important step is the physics simulation. Mathematical equations are used to calculate the state of the model in the next time step. This is usually a different shape or position due to a certain force.

Between the in- and output data are the controllers and monitors. Just like input data the controller can control the model. The difference is that a controller can use information from the previous time step to alter the input data. Monitors are essentially the same but there function is solely to monitor certain outputs in between time steps.

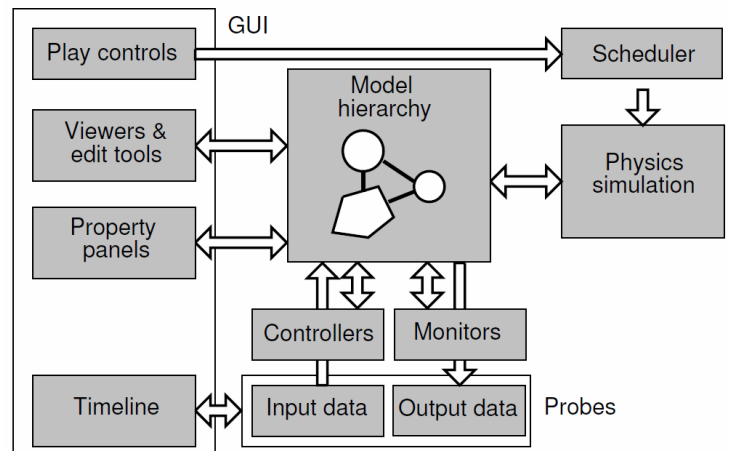


Figure 32: flowchart illustrating the system workflow in ArtiSynth. Image acquired from Lloyd et al. (2012)²⁶.

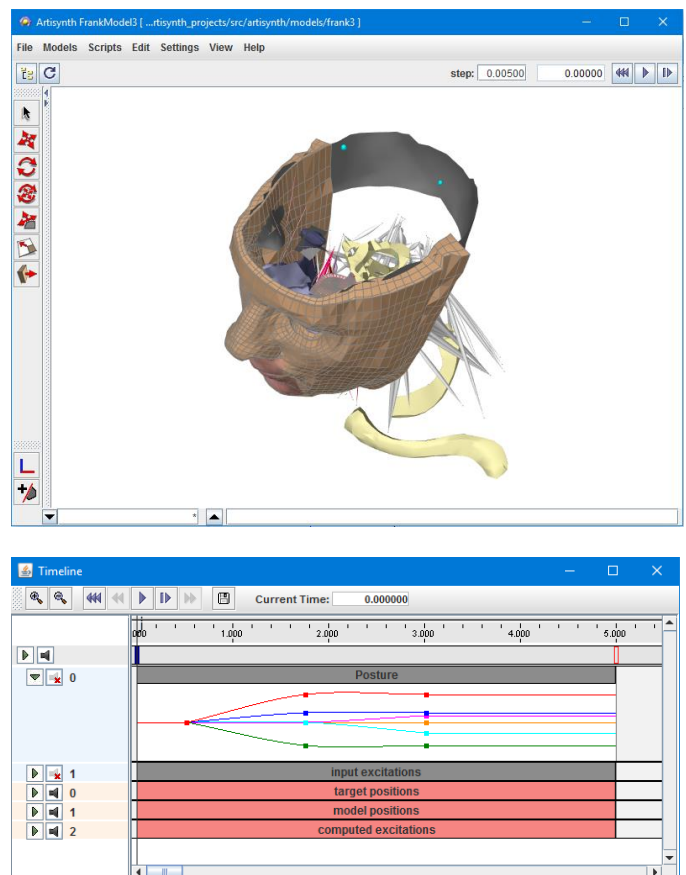


Figure 33: The ArtiSynth GUI consist of a main screen (upper image) and a timeline (lower image). A properties panel can be added to every individual model and host properties specific for that model.

Creating a biomechanical model in ArtiSynth

Creating models in ArtiSynth is usually done in code, using an integrated development environment (IDE) such as NetBeans or Eclipse. It is important to know that ArtiSynth has a clear component hierarchy. The component at the bottom of this hierarchy can use most of the components that are higher in hierarchy. At the top is the RootModel. This model contains all models including components that interact with the simulation such as: Controllers, monitors, property panels and probes. The Virtual surgery tongue model for example is an instance of FemModel named VS_Tongue, which contains the FEM structure, Muscles bundles, FEM makers (anchor points) and more. These last components are actually containers for even more components. Components can be accessed by following the path to this component, for example: /RootModel/models/VS_Tongue/Musclebundles/STY_L

Because VS_tongue is an instance of FemModel everything for the creation of a FEM Model is already in place. A particular model is built by providing information about the positioning of structures and values of properties. Programs like eclipse are especially useful when building a model because they provide the user with information about the contents those components.

Physical Simulation: Forward modelling

To advance the biomechanical model forward in time physical simulation is needed. At each time step a second-order ordinary differential equation (ODE) that is a result of the physics of the mechanical system need to be solved. FEM models in ArtiSynth use a lumped mass model as these are easy to connect to ridged bodies or mass-spring (e.g. muscle fibre bundles) components. The formula used is newton's second law:

$$\mathbf{M}\dot{\mathbf{u}} = \mathbf{f}(\mathbf{q}, \mathbf{u}, t) \quad (42)$$

With \mathbf{M} the composite mass matrix, \mathbf{q} the positions of the dynamic components, \mathbf{u} the velocities, $\mathbf{f}(\mathbf{q}, \mathbf{u}, t)$ the force of all force effector components and t the time. Bilateral and unilateral constraints are needed to solve the equations. Bilateral constraints include rigid body joints, Fem incompressibility and point-surface constraints. Unilateral constraints include contact and joint limits. Bilateral constraints are given as $\mathbf{G}(\mathbf{q})\mathbf{u} = 0$, unilateral as $\mathbf{N}(\mathbf{q})\mathbf{u} \geq 0$

Solving the ODE

Integrating 1 and 2 in ArtiSynth can be done using explicit and implicit integrators. When FEM body is present usually an implicit integrator is used with an eye on performance. Models using FEM are usually stiff and are therefore an implicit integrator is requested. The integrators that can be used are:

ForwardEuler

First order forward Euler integrator. Unstable for stiff systems.

SymplecticEuler

First order symplectic Euler integrator, more energy conserving than forward Euler. Unstable for stiff systems.

RungeKutta4

Fourth order Runge-Kutta integrator, quite accurate but also unstable for stiff systems.

ConstrainedBackwardEuler

First order backward order integrator. Generally stable for stiff systems.

Trapezoidal

Second order trapezoidal integrator. Generally stable for stiff systems, but slightly less so than ConstrainedBackwardEuler.

Solving the equations using is trapezoidal integrator in explained in J.E. Lloyd et al.²⁶

Friction and damping

Artisynth uses a couple of damping techniques such as Columb friction and Box friction that are discussed in the Artisynth reference manual⁵¹. Also translational damping, rotary damping and damping terms embedded in for example muscle fibres are available. For FEM models Rayleigh damping is used in the form of:

$$\mathbf{D}_F = \alpha \mathbf{M}_F + \beta \mathbf{K}_F. \quad (43)$$

Where \mathbf{D}_F is the mass matrix of the FEM nodes, \mathbf{K}_F is the FEM stiffness matrix, α is the mass proportional Rayleigh damping coefficient. β is the stiffness proportional Rayleigh damping coefficient.

\mathbf{D}_F will be embedded in the system matrix when solving the ODE.²⁶

Inverse modelling

Inverse simulations are used to compute muscle activations that are needed for a certain movement in a forward simulation. The inverse simulation used in ArtiSynth is based on the material of I. Stavness³⁷ The input in this case is a certain position in space for a certain part of the tongue. The muscle activation combination to achieve that position is the output of the calculation. Quadratic programming is used to find the muscle combination for a certain movement. Because there are different muscle combinations to achieve the same movement a criteria is needed to come to a single solution. In this case a "cost function" is used. This means, in this specific case, that is the muscle combination with the lowest combined muscle excitations have to be found. The generic term for the cost function based on the Dantzig's LCP pivoting algorithm is:

$$\operatorname{argmin}_{x \in \mathbb{R}^n} \left\{ \frac{1}{2} x^T Q x - x^T L \right\}, Ax \geq b, A_{eq} x = b_{eq} \quad (44)$$

With Q a nxn real symmetric matrix, L the linear n-dimensional Colum vector. A , A_{eq} , b_{eq} , b are (in) equality constraints. x are the muscle activations and \mathbb{R}^n is set to $[0,1]$, because x can be between 0 and 1. Different cost terms have to be combined to calculate the complete cost function. The cost functions that ArtiSynth uses are: A motion target term, which is responsible for the tracking behaviour as it tries to minimize the velocity between the target and the object. An L2 regularisation term is used to penalize the L2-norm (Euclidian distance) of the vector from the activation signals. This prevents simultaneous activation antagonist muscles that result in no motion. A damping term is used to penalize substantial changes in activations to smooth the overall movement of the FEM model.

Appendix F. PROSPECTIVE RANGE OF MOTION STUDY

A biomechanical model may in theory be the most detailed way to predict postoperative motion of the tongue and thus function, but it is certainly not the only way. van Dijk et al.²⁴ started two studies in which patient tongue range of motion (ROM) is used as a measurable indicator for functional outcome. This ROM is measured with a validated method using a 3D camera system¹⁵. The first study with the use of this camera focusses on finding a correlation between tumour volume and postoperative range of motion of the tongue. The second study examines if a large preoperative ROM is an indication for postsurgical function preservation. Pre and post-operative motion data from this study is also used for the validation of the virtual surgery model. With the use of The 3D camera system the location of the tongue is determined during the following manoeuvres:

- Elevation
- Depression
- Left
- Right
- Protrusion

Inclusion criteria:

Subjects with an age ranging from 18 to 90 years with a squamous cell carcinoma that are scheduled for surgical treatment.

Exclusion criteria:

- Patients that are not able to fill in questionnaires
- Palliative treatment
- History of oral or oropharyngeal cancer
- Radiotherapy on tongue surface

ROM acquisition

The 3D camera system consist of 3 camera's fixed in an angle of 20 degrees and a distance of 15 cm to each other (Figure 34). The cameras are then calibrated using an object consisting of 27 beads that are arranged on a 3x3x3 orthogonal grid. For the information on tongue position a reference point is places on the tongue, the tip of the nose, the naision and midline of the eyes(Figure 35).

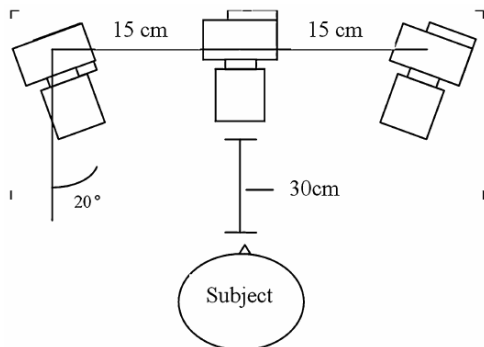


Figure 34: Illustration of camera setup used during the ROM measurements.

The first step in the offline analysis is the calibration of the interdental papilla with the markers on the face. This is because

the distances will be expressed in the distance between tongue tip and interdental papilla. In the frames where maximal tongue excursion is achieved all markers and the tongue tip will be manually selected for all cameras (Figure 35). Using this information the 3D coordinates of these points can be calculated.

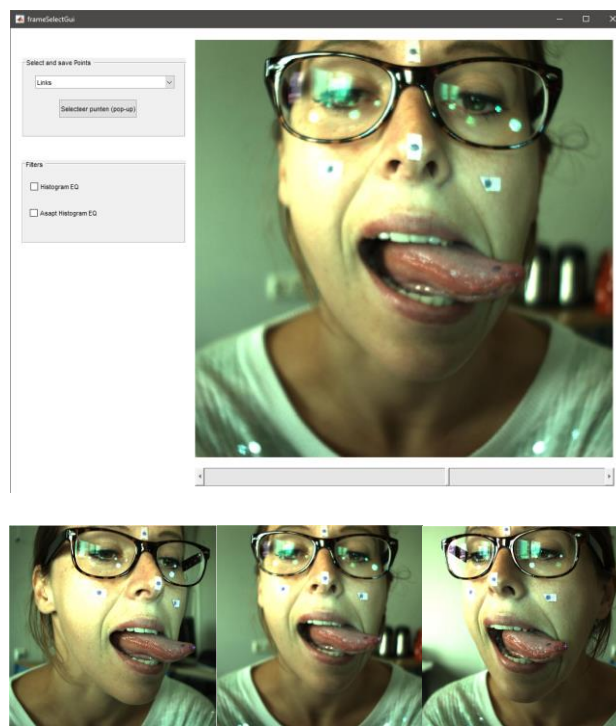


Figure 35: upper image: Matlab program used to select the reference points on the face and tongue. lower images: The same image from 3 different camera's.

The root mean square error of this 3D of this operation is 0.73 mm.¹⁵ Interrater variability had an interclass correlation(ICC) of 0.99 and an intrarater variability of 0.95. The test-retest variability was 0.93¹⁵.

Questionnaires

In addition to the ROM measurements also questionnaires regarding Quality of life and speech handicap will be filled in. The questionnaires are:

- The Speech Handicap Index⁵²
- EORTC-H&N 35 quality of life questionnaire will be used to measure oral transport issues.
- A performance status scale for head and neck cancer patients.⁵³
- 2 questionnaires about how patient perceive their own speech and voice validated in earlier studies in the NKI.^{54,55}
- The M.D. Anderson Dysphagia Inventory. This is a validated 20-point self-administered symptom-specific outcome instrument for dysphagia in head and neck cancer patients⁵⁶. This is used to assess the amount swallowing problems

In the first results can be seen that healthy subjects generally have symmetrical lateral movement of the tongue. The lateral movement in tongue cancer patients significantly differ. The other two ongoing studies already show that tumour volume is probably a better prognostic factor for postoperative tongue range of motion than tumour stage.

Pre and post range of motion measurements are also used as input and/ or validation of the biomechanical model. Only the Euclidian distances that are measured pre and postoperative will be used in the validation of the biomechanical model. Parts of the questionnaires that are used in prospective range of motion study are also used in the surgeon versus biomechanical model in Appendix G.

Appendix G. SURGEON VERSUS BIOMECHANICAL MODEL

In 2009 A. Kreeft¹⁴ showed that there is no absolute consensus with regard to functional results for most treatments in oral oropharyngeal cancers. This is what led to the idea of virtual therapy. A biomechanical model could help surgeons by predicting functional loss. But when would this system be beneficial in clinical practice? The answer to that question is actually quite simple: The moment when the system is better in predicting functional loss than the actual surgeon.

It is expected that it will take some time before we reach this point but because of the ongoing studies of van Dijk et al.²⁴ with the 3D acquisition of pre and post motion data of patient (Appendix F), it is beneficial to act now.

Prospective method

In the studies of van Dijk et al.²⁴ a lot of questionnaires are filled in to assess the pre and postoperative quality of life, speech issues and other handicaps. In this small study a selection of these questions will be asked to the surgeon pre-operative. The surgeon is asked to fill in their prediction for the patients answers to these questions six months postoperatively. Some questions used in the questionnaires in the study of van Dijk et al.²⁴ are entirely subjective and therefore not included in this questionnaire. Both the surgeon that performs the surgery and the surgeon that last saw the patient at the outpatient clinic will be asked to fill in this questionnaire.

Retrospective method

The inclusion of patients of van Dijk et al.²⁴ started in 2014 while the acquisition of questionnaires from surgeons started at the end of 2015. Because of this a lot of patients from the ROM study are not included in the prospective method. By using a retrospective method these patients could still be included. In retrospective research, all MRI images of the patients already included in the ROM study will be examined by several surgeons. On the basis of preoperative MRI images a prediction has to be made for the patients postoperative functional outcome. As the MRI images will be anonymised it will be unlikely that the surgeon will remember the outcome of this patient.

Results & discussion

At this moment the amount of data that is available from patients 6 months postoperatively is too little to say something about the prediction of functional outcome by the surgeons. Surgeons find it difficult to give a prediction about the functional outcome mainly because the surgeon in the outpatient clinic is not the same surgeon that performs the surgery. So the surgeon who performs the operation has only just seen the patient and the patient is not able to perform any test. Because the meeting at the out-patient clinic is usually long ago, surgeons are not sure about these predictions either. Also because the limited availability of preoperative drawings of the surgical resections it is almost impossible to validate the right location of surgery in the biomechanical model. The method for validating the biomechanical model has to be improved in order to compare it with the prediction of the surgeon. Surgical drawings have to be made and it would be better to fill in the questionnaire right after a consult on the out-patient clinic. Maybe the best option would be to find a way to create the virtual surgical resections in a retrospective way by analysing MRI images.

Not all questions from the Range of Motion study are used. Only selected questions. The used questionnaires are:

- 3 invalidated questions
- All questions from the validated NKI studies^{54,55}
- 4 questions from the MD Anderson QOL questioner.⁵⁶
- All questions from the performance status assessment.⁵³
- In addition to the standard questionnaire there are 2 questions about the direction of motion impairment of the tongue. These are not validated but are expected to be a more exact compartment as the primary outcome of the biomechanical model will be an impairment of motion in a certain direction.

Below is the complete questionnaire used. The questionnaire is in Dutch.

Het antwoord van de patiënt (preoperatief) is ingekleurd. Geef met een kruis aan wat u verwacht dat de patiënt postoperatief (6 maanden later) zal invullen.

Situatie na 6 maanden		
Is de stem en spraak zoals het is geweest?	Ja	Nee
Heeft de patiënt logopedie nodig?	Ja	Nee
Heeft de patiënt een voedingszonde nodig?	Ja	Nee

	Spraak 6 maanden na operatie	Slecht	Matig	Redelijk	Goed
1	verstaanbaarheid?	1	2	3	4
2	volume van de stem?	1	2	3	4
3	klank van de spraak?	1	2	3	4
4	snelheid van de spraak?	1	2	3	4
5	verstaanbaarheid over de telefoon?	1	2	3	4

	Functie 6 maanden na operatie	Helemaal niet	Een beetje	Nogal	Heel Erg
5	Heeft de patiënt moeite met slikken bij drinken?	1	2	3	4
6	Heeft de patiënt moeite met slikken bij het eten van gepureerd voedsel?	1	2	3	4
7	Heeft de patiënt moeite met het slikken bij het eten van vast voedsel?	1	2	3	4
14	Heeft de patiënt problemen met smaakvermogen?	1	2	3	4

	Functie 6 maanden na operatie	Nooit	Bijna nooit	Soms	Bijna altijd	Altijd
15	Moet de patiënt moeite doen om te spreken	1	2	3	4	5

Performance Status Assessment, 6 maanden na OK

Eten in het openbaar	
100	Geen beperkingen qua plaats, soort eten of gezelschap. (uit-eten gaan is geen probleem)
75	Geen beperkingen qua plaats/locatie, maar wel beperkt in het soort eten in het openbaar (eet overall, maar past soort eten aan naar minder risicovolle gerechten waarbij minder wordt geknoeid of een kleine kans op verslikken)
50	Eet alleen in gezelschap van vertrouwde personen en op een select aantal (vertrouwde) plaatsen
25	Eet alleen thuis in aanwezigheid en in gezelschap van vertrouwde mensen
0	Eet altijd alleen
Verstaanbaarheid van de spraak	
100	Altijd verstaanbaar
75	In de meeste gevallen verstaanbaar, soms is een herhaling nodig
50	Normaal gesproken wel verstaanbaar, een-op-een contact is wel nodig
25	Moeilijk te verstaan
0	Nooit te verstaan, gebruikt soms pen en papier
Beperkingen in het dieet	
100	Volledig dieet, geen restricties
90	Pinda's, noten
80	Al het vlees
70	Wortels of selderij
60	Droog brood en crackers
50	Zacht, makkelijk te kauwen voedsel (zoals: Macaroni, (door)gekookte groenten, vis, kleine stukjes vlees, zacht fruit)
40	Zacht voedsel waarbij niet gekauwd hoeft te worden (aardappelpuree, appelmoes, pudding)
30	Gepureerd voedsel
20	Warme dranken/vloeistoffen
10	Koude dranken/vloeistoffen
0	Sonde voeding

Positie van de punt van de tong in rust, 6 maanden na OK (combinaties mogelijk, kruis aan wat van toepassing is)

- Geen
- naar boven
- naar onderen
- Naar links
- Naar rechts
- Naar achteren

Richting bewegingsbeperking punt van de tong, 6 maanden na OK (combinaties mogelijk, kruis aan wat van toepassing is)

- Geen
- naar boven
- naar onderen
- Naar links
- Naar rechts
- Naar achteren